

The Pennsylvania State University
The Graduate School
Department of Aerospace Engineering

**DESIGNING FOR THE SPACE ENVIRONMENT VIA TRADE SPACE
EXPLORATION**

A Thesis in
Aerospace Engineering

by
Christopher Binz

© 2010 Christopher Binz

Submitted in Partial Fulfillment
of the Requirements
for the Degree of

Master of Science

May 2010

The thesis of Christopher Binz was reviewed and approved* by the following:

David B. Spencer
Associate Professor of Aerospace Engineering
Thesis Advisor

Deborah A. Levin
Professor of Aerospace Engineering

George A. Lesieutre
Professor of Aerospace Engineering
Head of Department of Aerospace Engineering

*Signatures are on file in the Graduate School

ABSTRACT

The focus of spacecraft design has long been on cost efficiency. Many options exist that will fulfill the mission requirements, but the best design is the one which maximizes the return while minimizing the cost. The industry has a number of ways to optimize the design process, but this thesis suggests a new method.

The traditional design process includes consideration of space environment effects, but normally these are secondary concerns. This work brings these effects – specifically contamination, radiation, and atomic oxygen attack – to the forefront of the process. An Earth-sensing satellite in low Earth orbit is used as a design example.

A basic model is developed in Microsoft Excel, and includes thermal, power, optics payload, and thruster/propellant design issues. In the thermal model, a simple lumped approximation is used, and the effects of thruster plume contamination on the thermal control surfaces are accounted for. The solar panel lifetime is estimated using a model for degradation due to the radiation environment as well as thruster contamination. The optics payload performance is a function of contamination and spacecraft glow. Atomic oxygen erosion of the selected thermal control material is also used as a lifetime estimate.

The model allows the designer to input somewhat high-level design variables, such as the dimensions of the spacecraft, and the selection of thermal control material and thrusters; and calculates estimates for relative lifetime, cost, and performance. It is then linked with Penn State's Applied Research Lab's Advanced Trade Space Visualization (ATSV) software, which allows designers to use the "design by shopping" paradigm by

providing visual steering tools. This setup is used to search for optimal designs in several different cases.

The model generally converges in less than 10,000 designs, with many cases converging in fewer than 5,000. The visualization tools easily show trends such as the primary limiting lifetime factor (solar arrays), the effects of a limited propellant budget, and the groups of materials which are best suited for this problem. In addition to showing the single optimal design, the Pareto sets are shown as well. The industry trend towards smaller spacecraft is reflected here, with most preferred designs on the order of 30% of the maximum allowable volume. Feasible designs are found for most thermal materials, and all propellant options.

This combination of designing specifically for space environment effects and using visual steering to aid in the optimization process creates a new way for designers to approach the problem.

TABLE OF CONTENTS

LIST OF FIGURES	vii
LIST OF TABLES	ix
ACKNOWLEDGEMENTS	x
Chapter 1 Introduction	1
Chapter 2 Literature Review	3
2.1 Trade Space Visualization	3
2.2 The Space Environment	6
2.2.1 Thermal Environment	7
2.2.2 Contamination	8
2.2.3 Radiation Environment	9
2.2.4 Atomic Oxygen	10
2.3 Current Design Process	12
2.4 Problem Statement	13
Chapter 3 Model Development	14
3.1 Spacecraft & Mission Description	14
3.2 Inputs, Outputs, & Constraints	15
3.3 Thermal Balance	16
3.4 Solar Array Sizing	19
3.5 Contamination	21
3.5.1 Amount of Propellant	22
3.5.2 Residence Time	23
3.5.3 Film Distribution	24
3.5.4 Effects	25
3.6 Atomic Oxygen Effects	25
3.7 Glow	27
3.8 Objective Evaluation	28
3.8.1 Lifetime	28
3.8.2 Optics Performance	29
3.8.3 Cost	30
Chapter 4 Analysis	31
4.1 Objective Sets	32
4.2 Procedure	34
4.3 Single Objective Optimization	35
4.3.1 Lifetime	35

4.3.2 GLOW	39
4.3.3 Cost.....	41
4.4 Multi-objective Optimization	42
4.4.1 Low Cost, High Quality	43
4.4.2 Long Lifetime, High Quality.....	45
4.4.3 Long Lifetime, Low Cost	50
4.4.4 Optimize All Objectives	52
4.5 Case Comparison.....	58
Chapter 5 Conclusions and Future Work.....	61
5.1 Conclusions.....	61
5.2 Suggestions for Future Work.....	63
References.....	65

LIST OF FIGURES

Figure 2.1: Applied Research Lab Trade Space Visualizer (ATSV).....	5
Figure 2.2: MSISE-90 atomic oxygen number density.	11
Figure 3.1: A Galaxy XII communications satellite, similar to the type of spacecraft being designed in this problem.....	15
Figure 3.2: An outline of the basic form of the model used.	16
Figure 3.3: Contrasting design methods for solar array sizing.	20
Figure 4.1: Objective function resulting from preference controls set in Figure 4.2...	31
Figure 4.2: ATSV brush preferences control window.	33
Figure 4.3: Cost vs. Lifetime plot, maximum lifetime case.....	36
Figure 4.4: Cost vs. Lifetime, maximum lifetime case, zoomed in to the best designs.	38
Figure 4.5: Parallel coordinates plot, minimum GLOW case.....	39
Figure 4.6: GLOW vs. Lifetime plot, zoomed in to area of interest.	40
Figure 4.7: Cost vs. GLOW plot, both minimized.....	44
Figure 4.8: GLOW vs. Lifetime scatter plot, high Lifetime and performance case, Pareto front highlighted.	47
Figure 4.9: Parallel coordinates plot for long life, high performance case.....	48
Figure 4.10: GLOW vs. Lifetime, with Cost used as brush preference.....	49
Figure 4.11: Cost vs. Lifetime plot, Pareto designs highlighted.....	51
Figure 4.12: Discontinuity in design space, three objective case.	53
Figure 4.13: Pareto set highlighted, color showing preference.	54
Figure 4.14: Isosurface at propellant budget-caused discontinuity.	55
Figure 4.15: Parallel coordinates plot for three-objective case.....	56
Figure 4.16: Best design highlighted.	57

Figure 4.17: Parallel coordinates plot showing the thermal control material and thruster selections.	59
Figure 4.18: Cost, GLOW, and Volume across each objective set.....	60

LIST OF TABLES

Table 3.1: Terms used in the thermal rate equations	18
Table 3.2: Efficiency terms used for solar panel calculations.	21
Table 3.3: Other values used for solar panel calculations.	21
Table 3.4: Reaction efficiencies of various spacecraft thermal control materials.	26
Table 4.1: Outline of the various objective preference sets explored.	34
Table 4.2: Maximum lifetime design details	38
Table 4.3: Minimum GLOW design details	41
Table 4.4: Minimum Cost design details	41
Table 4.5: Baseline objective values.....	42
Table 4.6: Minimum GLOW, Minimum Cost design details	45
Table 4.7: High Lifetime, high performance design details	50
Table 4.8: High Lifetime, low cost design details	52
Table 4.9: Three-dimensional optimization design details.....	57

ACKNOWLEDGEMENTS

Foremost, I would like to thank my advisor, Dr. David Spencer, for providing me with invaluable support and guidance through this process. I would also like to thank Dr. Deborah Levin, who provided her technical expertise on the subject of the space environment.

The ATSV research group proved to be an excellent forum for ideas and feedback, and I thank Dr. Timothy Simpson, Gary Stump, and every other member for their support.

Finally, I want to thank my family, especially my parents, who made my education possible, and to whom I credit all of my success thus far; and my girlfriend, Laura, for providing unwavering support and motivation throughout the years.

This work has been supported by the National Science Foundation under Grant No. CMMI-0620948.

Chapter 1

Introduction

Engineering design can be a very complicated process, and this holds especially true for spacecraft design. Subsystems are coupled with many other components. As a result, and as with most engineering design problems, there always exists a space of many acceptable designs. This is where optimization becomes necessary. The design space is explored, important traits are characterized, and the “best” design (or set of designs) is chosen.

As a result of the often large design space, automation is usually required for optimization problems. Frequently, the optimization process consists of a “black box” algorithm which generates many designs and decides which are the best based on pre-defined criteria. A different approach is used here. With trade space visualization, the designer is kept in the optimization loop, allowing him or her to make decisions on the fly, and even to change the relative importance of objectives. This emerging paradigm, known as design by shopping, is discussed in detail in Section 2.1. This procedure is very well-suited for spacecraft design optimization, because the complexity of space systems often does not allow the designers to have a clearly-defined, static set of objectives beforehand.

Since spacecraft generally represent a significant investment, designers often try to maximize cost efficiency. The operational lifetime of the vehicle is desired to be as

high as the budget will allow, without sacrificing performance or capability. This need for long-life spacecraft is one of the motivations for this work.

Because the space environment can have a significant effect on the lifetime of a spacecraft, this work uses spacecraft/environment interactions as the main driver for optimization. This work quantifies the estimated cumulative effects of the space environment not only on the lifetime of the spacecraft, but also the performance of any onboard optical payload. In addition, the launch cost is estimated from the approximate size and components utilized in the design. The underlying physics of the spacecraft/environment interactions are discussed in Chapter 2, and the model developed to quantify these effects is discussed in Chapter 3.

The model is linked with the ARL Trade Space Visualizer (ATSV), a trade space exploration tool developed at the Pennsylvania State University, and Chapter 4 presents the findings for different sets of objective weights. Conclusions and suggestions for future work are presented in Chapter 5.

Chapter 2

Literature Review

2.1 Trade Space Visualization

Optimization of complex systems is one of the most common problems in engineering. First, the problem is articulated, and mathematical models are developed. System drivers and objectives must be identified early in this process in order to create an accurate, effective model. These models is used to create a set of designs, which can then be compared to one another. The traditional optimal design approach involves “scoring” specific designs according to a set of predefined evaluation criteria [1]. The design space is populated, and whichever design has the highest (or lowest, depending on the case) score is chosen as the optimum. The score is generally a weighted combination of several objective values, otherwise known as an objective function. The weights are subjective and are chosen at the beginning of the design process. These are selected according to the relative importance of each individual objective. This process forces the designer to commit to a set of objective weights at the beginning of the process.

More recently, Balling has introduced the “design by shopping” paradigm [2]. Here, designers are allowed to change the importance of each objective after the design space has been populated. This means that the designer no longer has to commit to an “ideal design” early in the process. The designer can now formulate a set of optimal design criteria *a posteriori*, after exploring the design space with visualization, as

opposed to *a priori* [3]. This research was the motivation that led to the Applied Research Lab Trade Space Visualizer (ATSV) [4], which is the tool used in this research.

ATSV is an engineering tool that allows the user to search for an optimal design with visualization tools and the ability to quickly identify Pareto sets. A Pareto set is the group of designs which represent the optimal trade-offs between two or more objectives. The models are developed in separate programs, such as Microsoft Excel, and then linked with the Java-based ATSV. Once linked, ATSV generates a design space by driving the models using one of several samplers. In addition to the Basic Sampler, which randomly generates designs, ATSV also includes a Pareto Sampler (generate designs close to the Pareto front), Preference Sampler (generate designs based on design preferences and objectives), Attractor Sampler (generate designs close to a specified point in the design space), and the Point Sampler (generate nearby designs by holding all but one variable constant). One of the most powerful features of ATSV is its ability to efficiently visualize the design space in a large number of ways, including multi-dimensional plots (up to 8 dimensions using variables like color, transparency, and size), parallel coordinates, and histograms. All visualizations are updated in real-time, allowing the user to see any relationships between objectives and/or variables. Figure 2.1 shows the interface of ATSV, along with several of its visualization capabilities.

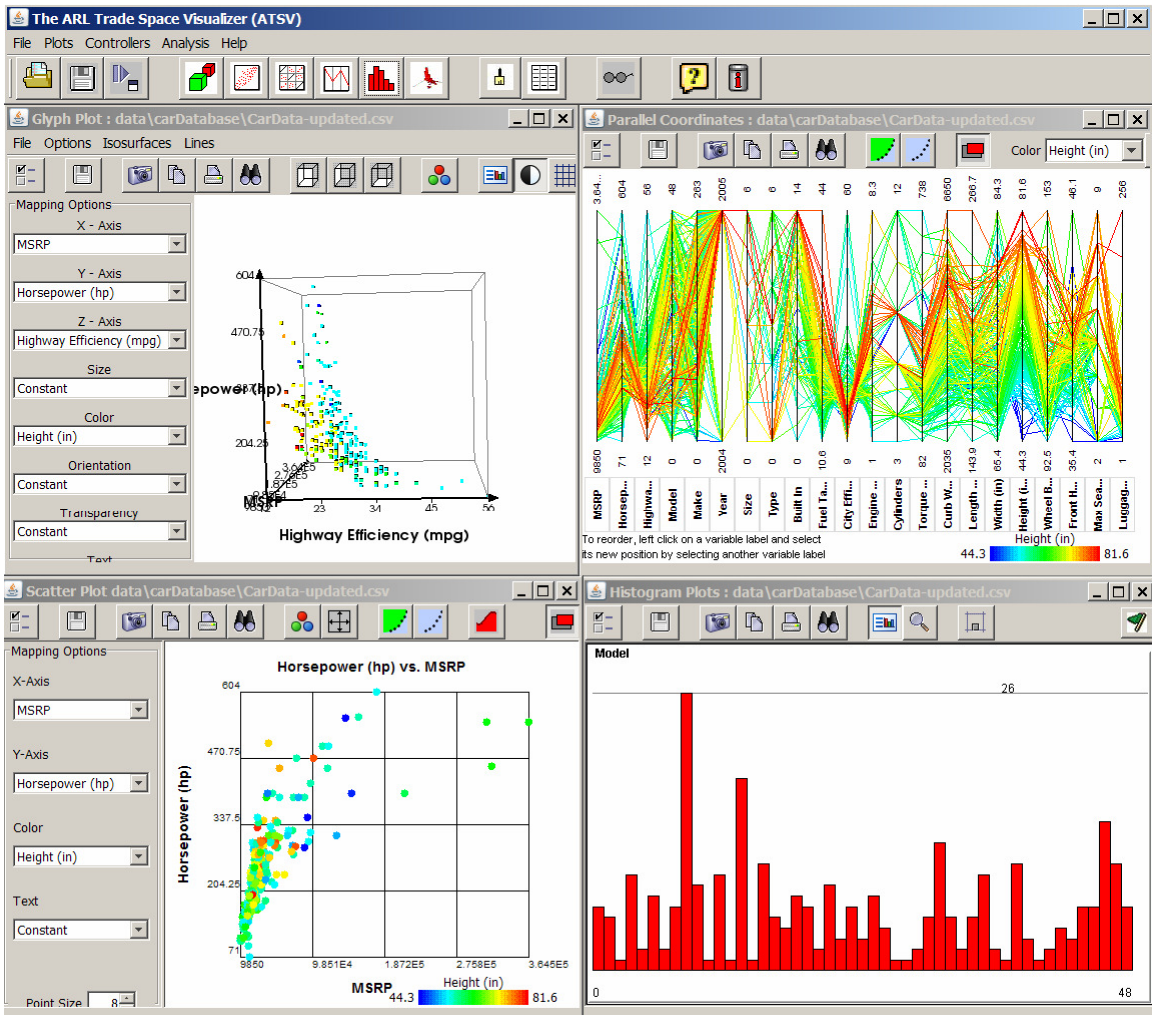


Figure 2.1: Applied Research Lab Trade Space Visualizer (ATSV).

This method of optimization is well-suited for a spacecraft design project. In its early stages, it may be nearly impossible for a designer (or team of designers) to know exactly what they are looking for *a priori*, because of the implicit complexity of spacecraft systems. ATSV allows designers to easily explore and visualize highly-coupled systems inherent in spacecraft design, as well as avoid unintended consequences of particular combinations of variables, such as higher-than-expected levels of

contamination. In addition, the flexibility of ATSV makes it suitable for both component-level and system-level design visualization and optimization.

In fact, this tool has been applied to several space mission design problems in the past. Stump, et. al. [5] used a satellite design problem to illustrate the use of ATSV. They developed a model which included common satellite design considerations, such as propellant type, reaction wheel selection, slew time, and wet/dry mass. Their work served largely to illustrate different design trades and the way they can be visualized with ATSV, and this thesis builds on this work by adding space environment effects to the design process. In addition to space vehicle design, Jordan [1] used ATSV to explore continuous-thrust orbital maneuvers. This reiterates the assertion that ATSV can be applied to a wide range of design problems, even those which may not seem immediately suitable for this type of analysis.

2.2 The Space Environment

Operating in the space environment presents several unique challenges. Problems such as maintaining a thermal balance in a vacuum and increased exposure to radiation are immediately apparent, while the issues of contamination, atomic oxygen, and atmospheric drag are perhaps less obvious. In this work, the model is limited to some of the most important problems for an Earth-sensing satellite. Thermal considerations, contamination due to thruster plumes, atomic oxygen attack, spacecraft glow, and degradation of solar panels due to radiation are all considered. In the following sections, each of these phenomena, as well as its effect on spacecraft, is explained. An important

note on the use of empirical models in this work: in addition to providing a way to simplify these models, often empirical models represent the current state of the art. This holds especially true for some forms of contamination and spacecraft glow where the physical mechanisms are not yet fully understood.

2.2.1 Thermal Environment

The importance of maintaining an acceptable temperature range within a spacecraft cannot be understated. Many spacecraft components, such as batteries, have a relatively narrow acceptable temperature range. Therefore, thermal considerations are one of the main design issues with most spacecraft. The main issue here is the fact that the spacecraft is operating in a vacuum. Therefore, heat transfer can only be accomplished through either direct contact or radiation. The spacecraft as a whole absorbs energy from direct solar exposure, reflected sunlight from the Earth (albedo), and infrared emissions from the Earth, while also producing internal heat as a result of power dissipation [6, p. 387]. The main mechanism for heat dissipation is simple radiation to space. Therefore, the radiative properties of the outer spacecraft surface becomes a main concern. The optical properties of the surface, particularly the absorptance, can change as a result of contamination, and this is modeled. Details of the thermal model used are explained in Section 3.3.

2.2.2 Contamination

Contamination occurs when material attaches (physically or chemically) to exposed spacecraft surfaces. Often this material is residue from either thrusters or material outgassing [6,7]. Thruster contamination occurs when propellant comes into direct contact with a surface, either through direct impingement of the flow or backflow. Outgassing is the result of trapped molecules in a material being released once exposed to a vacuum, and it generally happens over time. Materials are carefully tested for use on spacecraft, and generally a material must pass very strict and well-defined criteria set forth by the American Society for Testing and Materials (ASTM) in order to be used in the space environment [6, p. 296].

Thruster contamination is generally dealt with by making sure no thruster plumes intersect any sensitive spacecraft surfaces. However, because many thrusters have some amount of propellant that gets “backflown” (flows at an angle greater than 90° from the center line of the thruster) [8], propellant often does cause some degree of contamination.

In each of these cases, the amount of contaminant that will collect on a surface is dictated by the residence time. This refers to the amount of time a molecule will remain bonded, physically or chemically, to the surface. As a result, contamination is a time-dependent process. The method for estimating residence time is shown in Section 3.5.2.

Contamination affects the optical properties of the surface on which it condenses, specifically the absorptance. This affects the way the spacecraft radiates and absorbs heat, and as a result the thermal balance is upset by any significant changes. Particularly, if a contaminant film causes a significant increase in the absorptance of the spacecraft

surface, the amount of absorbed energy may result in a temperature above the allowable threshold. Obviously this change in optical properties is complex, depending on the absorptance of both the surface and the contaminant across the entire spectrum. However, this has been simplified into an empirical model [9, p. 145], which is explained in Section 3.5.4. In addition to affecting the thermal balance of a spacecraft, contamination may also contribute to degraded solar panel power output. Although the operating temperatures of solar panels normally result in very low residence times (and thus very little contamination), Tribble and Haffner have contributed to the understanding of the faster-than-expected solar panel output degradation on GPS Block I satellites to contamination, brought about by photochemical reactions [10].

2.2.3 Radiation Environment

The surface of the Earth is largely protected from radiation by its magnetic field and, to a degree, its atmosphere [6, p. 243]. However, in space this protection is not available. In addition to radiation from the sun and other sources, the Earth's magnetic field traps a large amount of radiation in areas known as the Van Allen belts [7, p. 154]. Therefore orbiting spacecraft need to have significant onboard protection in order to mitigate the effects of radiation. Onboard electronics are particularly susceptible to radiation upsets, such as bit-flips in microprocessors [6, p. 270]. Redundant and resilient software is often required to protect against these failures, however physical shielding of sensitive components also plays a part. In addition, radiation damages solar cells in orbit. Radiation damages the n-p junction diode, effectively reducing the cell's efficiency [7, p.

182]. These losses can be significant: up to a 19% power loss in the first year alone [11, p. 339]. Solar panels may also be radiation hardened with clear coverings (which essentially absorb some radiation before it reaches the cell); however this does not totally eliminate the efficiency loss.

2.2.4 Atomic Oxygen

The atmosphere in low Earth orbit consists primarily of atomic oxygen and helium [6, p. 183]. Of these, atomic oxygen presents the biggest problems for spacecraft. Atomic oxygen number density varies according to the level of solar activity, but generally ranges from 10^6 to 10^8 particles per cm^3 for the altitude range in this example (450 – 550 km). Figure 2.2 shows atomic oxygen concentration as a function of altitude. The vertical axis, with units cm^{-3} , is the number density of oxygen atoms. Due to its high reactivity and impact energy, atomic oxygen causes certain spacecraft materials, especially polymers, to erode in orbit. The rate of erosion is quantified by the material's erosion yield. This value is determined for each material through testing, a large amount of which occurred on the Long Duration Exposure Facility (LDEF) spacecraft [7, p. 223], and is generally on the order of 10^{-24} cm^3/atom (Table 3.4 shows actual values for several tested materials). The relevant equations used for estimating the erosion yield are given in Section 3.6.

In addition to material erosion, atomic oxygen also plays a part in the spacecraft glow phenomenon. Although the mechanism is not completely understood, it is thought to be a result of the oxygen atoms interacting with the material on the leading edge of the

spacecraft [6, p. 185]. This interaction leads to an emission of visible light. The glow phenomenon has been observed on many spacecraft, and is known to be a function of altitude, likely because of the relationship between atomic oxygen density and altitude. For the purposes of this project, any light emission is treated as a detractor of the performance of the optical instruments on the spacecraft, and must be minimized. This glow effect is quantified in Section 3.7.

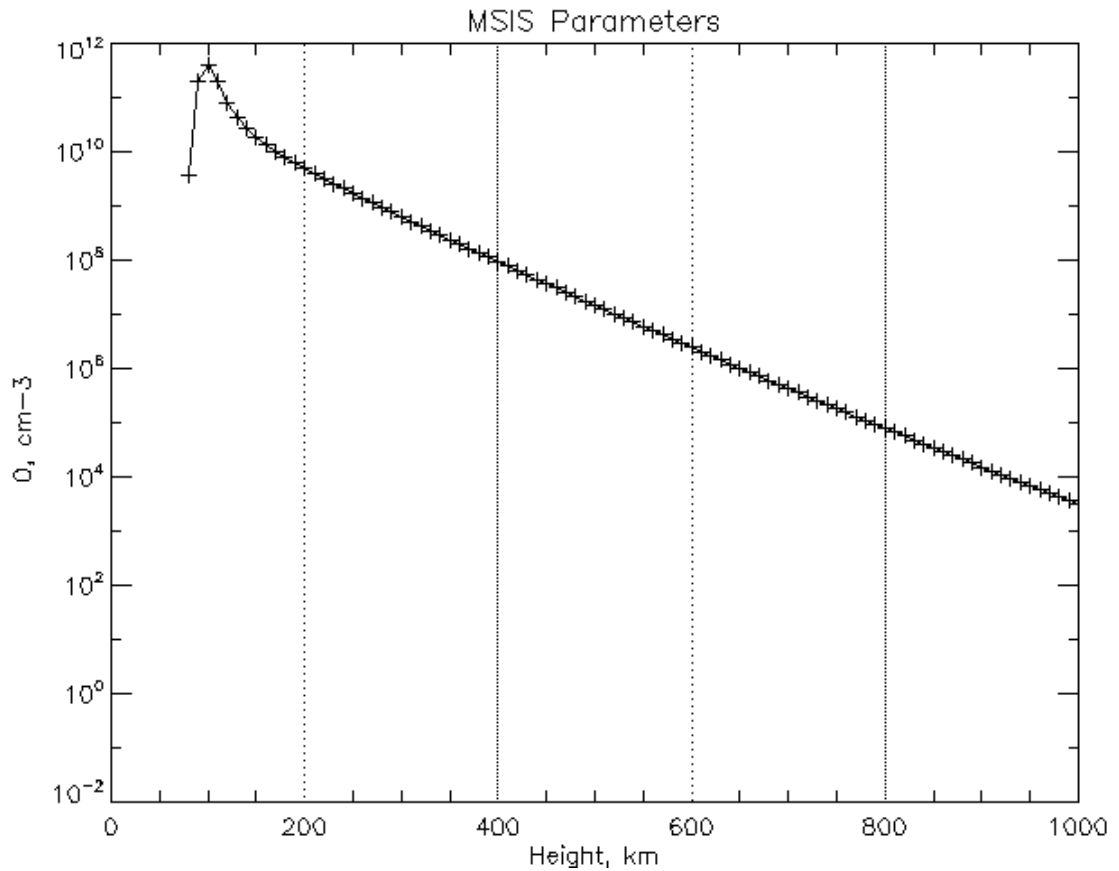


Figure 2.2: MSISE-90 atomic oxygen number density (produced via <http://ccmc.gsfc.nasa.gov/modelweb> on 12/08/09).

2.3 Current Design Process

The current spacecraft design process does involve space environment issues. However, the focus is generally on identifying and mitigating the effects of the space environment, rather than designing to minimize these effects [12]. General guidelines, such as identifying outgassing materials, calculating view factors for contamination control, and planning for solar array degradation due to contamination and radiation are in place currently [12,13, p. 221]. However, there is a host of spacecraft anomalies which suggest that these guidelines are not given the level of priority required [10,14]. The recent push towards small, low-cost, and high-reliability satellites [15] suggests that space environment effects need to be given a higher priority [16,17]. Specifically, the focus is being shifted towards radiation effects on on-board computers. While software and hardware redundancy and resiliency are important in the design of high-reliability, long-life spacecraft, this thesis features other space environment effects as primary drivers.

Because the design by shopping paradigm is a relatively young concept [2], it is not used as often as many other “black-box” optimization algorithms. As a result, the more traditional optimization methods are the most prevalent, especially in spacecraft design [18,19,20]. However, this process relies on designers knowing what they need *a priori*, which is often not the case, especially in the field of spacecraft design. An *a posteriori* approach seems much more suitable for this field. Trade space visualization lends itself well to this process, and it should be expected that it becomes more utilized over time.

2.4 Problem Statement

This thesis aims for two objectives: to experiment with making space environment effects the primary drivers in the spacecraft design process, and to apply visual steering and trade space exploration to the spacecraft design problem. To do this, an example Earth-sensing satellite design is studied. The main priorities for its design are low cost, high reliability and lifetime, and good sensor performance. The example sensor used is a wide-band optical sensor; because such sensors are usually maintained at cryogenic temperatures (in order to reduce noise), they tend to be very sensitive to contamination. A design model is developed, and this model is used to populate the trade space with spacecraft designs. Then, the Applied Research Lab's Trade Space Visualizer (ATSV) is used to visualize this multidimensional design space, and to select the optimum design (or set of designs) given a set of objectives.

Chapter 3

Model Development

The model that has been developed is not meant to be an all-inclusive, complete spacecraft design model. Instead, it focuses on specific aspects of the design, and is meant to provide estimations and comparisons to help guide the design process. It should be viewed as a “companion” model; to be run in tandem with another model or set of models to get a more complete view of the spacecraft design. Along with the more traditional thermal balance, solar array sizing, and thruster selection problems, the model includes contamination and atomic oxygen attack as primary design considerations. All calculations are made assuming worst-case conditions, so the resulting designs are far from the design limits. It is done entirely in Microsoft Excel, which is later linked to ATSV for design space exploration.

3.1 Spacecraft & Mission Description

The spacecraft example used in this thesis is assumed to be cubical, with two double-fold, extendable, rectangular solar panels. Since the example spacecraft is an Earth-sensing satellite, any optics are located on the nadir face. The orbit is assumed to be a high inclination, sun-synchronous, circular low-Earth orbit, chosen such that the spacecraft receives constant solar exposure, and typical for many Earth-sensing satellites [21,22]. A Boeing Delta II rocket is assumed to be the launch vehicle, and the cylindrical

fairing (3 meter diameter, 8.9 meter height [23]) gives constraints on the size and dimensions of the spacecraft. A typical example of this type of satellite is shown in Figure 3.1.



Figure 3.1: A Galaxy XII communications satellite, similar to the type of spacecraft being designed in this problem (Source: <http://claudelafleur.qc.ca/Spacecrafts-2003.html>, accessed 10/13/09).

3.2 Inputs, Outputs, & Constraints

The main input variables in the model are the dimensions of the spacecraft, the thermal control material (chosen from a database), and the thruster selection (chosen from a database). The material database includes the material's solar absorption coefficient (α), emissivity (ϵ), and reaction efficiency (where available) [9, p. 791-801]. The thruster database includes several representative thrusters, each with a different propellant and specific impulse [24]. The model also has a variable orbit altitude (225 – 650 km), however this is chosen at the beginning of the optimization process and kept constant throughout. The constraints on the dimension inputs are dictated by the launch vehicle fairing dimensions. The model produces relative lifetime and cost estimates as outputs, as well as a performance metric for the optics and a feasibility check. The

feasibility check ensures the current configuration satisfies the thermal balance, and that it will fit in the launch vehicle fairing. An overall look at the model and its components is shown in Figure 3.2.

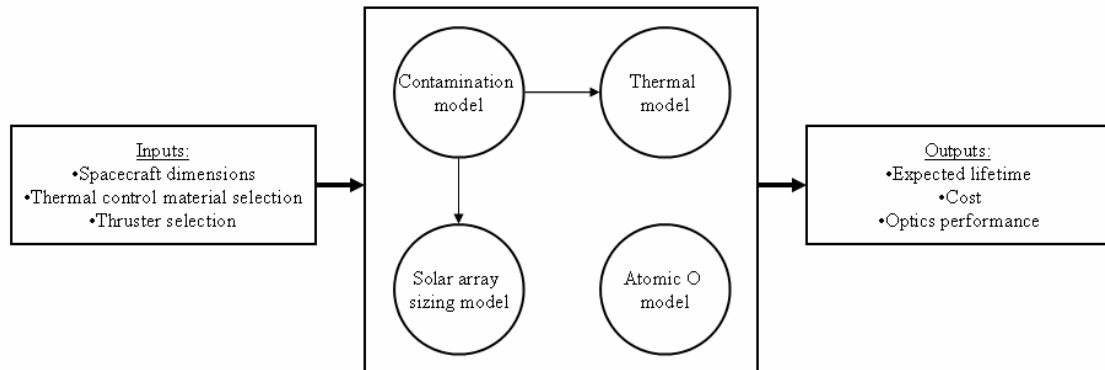


Figure 3.2: An outline of the basic form of the model used.

3.3 Thermal Balance

The thermal design portion of the model is based on a simple lumped approximation thermal balance. To simplify the design, the thermal control is designed to be completely passive (no on-board heaters, no thermal control louvers, etc.). An exception to this is the cooling system for the optics, which is assumed to be a self-contained refrigeration system (constant across all designs, and therefore not a design consideration in this work) [9, p. 84]. The majority of the spacecraft's outer surface is assumed to be covered in the selected thermal control material, while the inside of the spacecraft has a very high thermal conductivity. The result is that heat is able to be very evenly distributed throughout the spacecraft, which makes the lumped thermal model a

good approximation [25,26]. In addition, the fact that the chosen orbit is sun-synchronous with constant solar exposure also simplifies the problem significantly: since the spacecraft does not alternate between eclipse and non-eclipse conditions, the incident heat flux is nearly constant. The thermal balance equation used is shown in Equation 3.1 [6, p. 387]:

$$\dot{Q}_{Direct\ Solar} + \dot{Q}_{Earth\ IR} + \dot{Q}_{Earth\ Albedo} + \dot{Q}_{Space} + \dot{Q}_{Internal} = 0 \quad (3.1)$$

Here, the incident heat fluxes are direct solar exposure, earth infrared emission, and earth albedo (reflected sunlight) exposure. The fourth term in Equation 3.1 is for heat radiated to deep space, and the final term accounts for heat generated within the spacecraft (by electronics, for example). These thermal rate equations are presented below [6, p. 388-389], with Table 3.1 explaining the various terms.

$$\dot{Q}_{Direct\ Solar} = \alpha_s S_e A_p \quad (3.2)$$

$$\dot{Q}_{Earth\ IR} = \alpha_s \varepsilon_{IR} \dot{q}_{Earth} (1 - \cos \eta) A_p \quad (3.3)$$

$$\dot{Q}_{Earth\ Albedo} = \alpha_s \left(\frac{\dot{Q}_{a \rightarrow s}(h, \theta_s)}{A_p} \right) \left(\frac{A_b}{.34} \right) \left(\frac{S_e}{1395} \right) A_p \approx 0.20 \cdot \dot{Q}_{Direct\ Solar} \quad (3.4)$$

$$\dot{Q}_{Space} = -\varepsilon_{IR} \sigma A_s T_s^4 \quad (3.5)$$

Table 3.1: Terms used in the thermal rate equations [6, p. 374]

Term	Description
α_S	Absorption coefficient of the surface
S_e	Solar constant at Earth distance, mean value 1395 W m^{-2}
A_p	Cross-sectional area of sphere, m^2
ϵ_{IR}	Infrared emissivity
\dot{q}_{Earth}	Heat flux density of surface of Earth, 237 W m^{-2}
η	Maximum angle subtended by a sphere from a plate, $\sin \eta = R_{Earth} r^{-1}$
$\dot{Q}_{a \rightarrow s}$	Heat flux from Bond albedo surface to sphere
θ_s	Angle between Earth-Sun and Earth-Spacecraft vectors
A_b	Bond albedo of sphere, mean value 0.34
σ	Stefan-Boltzmann constant
A_s	Surface area of sphere, m^2
T_s	Temperature of surface, K

The spacecraft dimensions are given as an input to this section of the model, and the spacecraft is modeled as a sphere whose surface area matches those dimensions. The minimum and maximum allowable temperatures used are 263K and 313K respectively, taken from typical allowable ranges [11 (p. 374),27,28]. The other input variable is the thermal control material's emissivity ϵ . The material's standard emissivity is used here, since contamination does not significantly affect its value [7]. The internal heat generation is linked to spacecraft size based on an estimation using data from previous spacecraft [6,9,11 (p. 401),28]. Using the above equations for a hot and cold case (corresponding to the maximum and minimum allowable temperatures), the model calculates an allowable range for values of α . The worst-case contamination value for α is taken from the contamination portion of the model, and then compared to the calculated range. This is used as one of the "feasibility checks" in the main model.

3.4 Solar Array Sizing

The solar array sizing problem in the model essentially works backwards to give an estimate for the lifetime of an array given the appropriate specifications. Normally, the end of life power requirement is specified, as well as the projected lifetime, and the panels are designed and sized accordingly [27]. In this model, the maximum size is specified first, and, for a given end of life power requirement, the lifetime is estimated.

One of the main contributing factors to solar cell degradation is radiation effects. Radiation exposure to a solar cell leads to a loss of power output from the cell [7, p. 182-183]. Several models have been proposed for predicting the radiation loss for a given spacecraft [29,30], and the issue has been observed and studied on many actual missions [11 (p. 339),31]. For the purpose of simplicity, the degradation rate in the model is taken to be a constant 4% per year; although the actual rate is rarely constant, this estimate corresponds closely with both actual and estimated values for other spacecraft [31]. Contamination from thruster residue is normally not a significant problem because of the operating temperature of solar arrays [32,33]. However, there is evidence that contamination does occur [34], so it is incorporated into the model. The contaminant thickness is calculated (using the contamination model), and converted to a loss of efficiency [7, p. 57]. Still, contamination never amounts to more than about a 1% loss in efficiency.

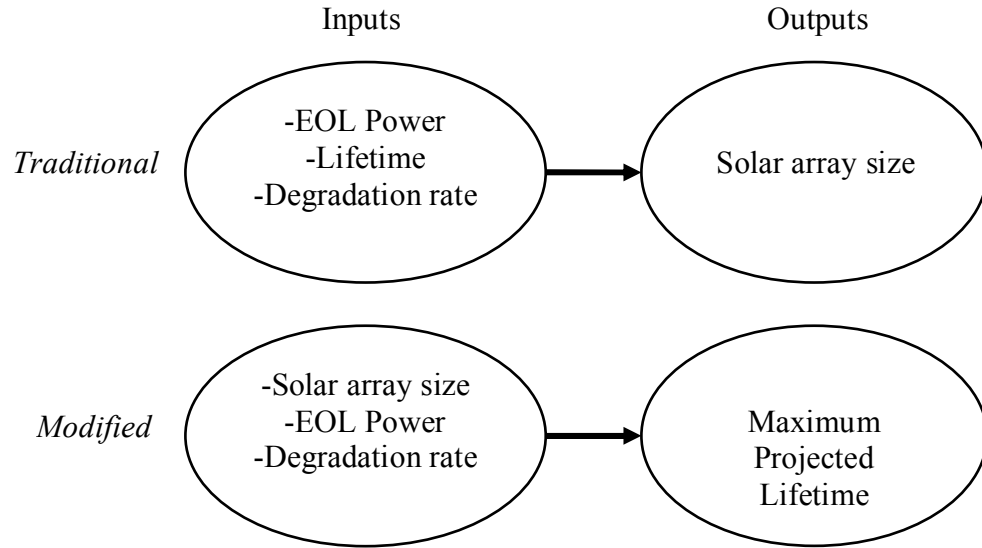


Figure 3.3: Contrasting design methods for solar array sizing.

The two main inputs to this model are the allowable size of the panels, and the approximate end of life power requirement. Both are directly related to the size and dimensions of the spacecraft. The array size is calculated assuming the two double-folded panels will be mounted on the two largest faces of the spacecraft. The end of life power is linked to the total size of the spacecraft, and is estimated for each design using a linear fit of data from previous spacecraft [11,25,35]. The main relationship used for calculations [7] is shown in Equation 3.6 below (S is incident solar flux [W/m^2], P is required end of life power [W], η is efficiency), where the value for η is calculated using Equation 3.7. The important values and individual efficiency terms used are given in Table 3.2 and Table 3.3.

$$A = \frac{P}{S\eta} \quad (3.6)$$

$$\eta = \prod_i \eta_i \quad (3.7)$$

Table 3.2: Efficiency terms used for solar panel calculations [11, p. 341-343].

Efficiency Term	Value Used	Efficiency Term	Value Used
UV Discoloration	0.980	Thermal Cycling	0.990
Cell Mismatch	0.990	Resistance Losses	0.980
Temperature Losses	0.890	Packing Efficiency	0.880

Table 3.3: Other values used for solar panel calculations [11, p. 346,36].

Description	Value used
Si Cell Efficiency	14.9%
Operating Temperature	50°C
Maximum Off Angle	6°

3.5 Contamination

Two of the major sources of contamination of a spacecraft in orbit are outgassing and thruster residue [6,7]. The majority of outgassing normally occurs only when the spacecraft is first put into orbit (within the first few weeks or months), and therefore any optically sensitive components are covered until the outgassing rate slows to an acceptable level [32]. For this reason, as well as for simplicity, the only contamination considered in this model is from thruster plumes. Essentially, the model estimates the amount of propellant that will come into contact with the spacecraft, and uses this to determine the average thickness of contaminant on each surface. This, in turn, affects most of the other subsystems in the model: the thermal balance, solar array efficiency, and optics' cleanliness/performance.

3.5.1 Amount of Propellant

The first step in this model is to estimate the amount of propellant which backflows from the thruster. To do this, first the total amount of propellant expelled over a certain time period needs to be calculated. The only thrusters this model considers are those used for spacecraft station-keeping, or drag compensation. Because this is a satellite in low Earth orbit, atmospheric drag is a significant concern. Deceleration due to drag on a satellite is given by the following equation [24, p.45]:

$$a_D = -\frac{1}{2}\rho\left(\frac{C_D A}{m}\right)v^2 \quad (3.8)$$

Because altitude change affects both atmospheric density, ρ , as well as orbital velocity, v , this is solved with an iterative method which uses incremental altitude changes (done with MATLAB here). The objective here is to get an estimate for the annual ΔV budget required for drag compensation. The term $\frac{C_D A}{m}$ is the reciprocal of the ballistic coefficient of the satellite. Because this changes for every design and every orientation of the spacecraft, the MATLAB iteration would have to be run for each new design. Since thousands of designs are generated for each optimization problem, this would slow things down significantly. Instead, an average value is used based on ballistic coefficients of previous spacecraft [37,38]. Typical ΔV values for satellites in low-Earth orbit range from about 5 m/s to 30 m/s per year, depending on the ballistic coefficient.

Given a specific value of ΔV for drag compensation, and taking into account the chosen thruster's mass flow rate (given by Equation 3.9), the amount of propellant

expelled from the thruster over any specified time interval can be found. The mass flow rate is calculated given the thruster's specific impulse (I_{sp}) and output force (F) as

$$\dot{m} = \frac{F}{I_{sp} g_c} \quad (3.9)$$

where g_c is the acceleration of gravity at the Earth's surface.

However, the vast majority of the propellant is expelled away from the spacecraft. Therefore the only propellant that will come into contact with the spacecraft is the unreacted, backflown propellant. The value used for this is 1% of the mass flow rate [8], however this is easily changed within the model if there is more specific data available for a particular thruster model.

3.5.2 Residence Time

Contamination is not a permanent thing. The contaminant stays on the spacecraft surface for only a certain amount of time. This is known as residence time, and it depends mostly on the surface temperature. Equation 3.10 gives residence time as a function of this temperature [6, p. 304-305]:

$$\tau = \tau_0 \exp\left(\frac{\Delta H}{kT}\right) \quad (3.10)$$

The residence time at nominal temperature, τ_0 , is estimated to be about 10^{-13} [6, p. 305], k is Boltzmann's Constant, T is the surface temperature in Kelvin, and ΔH is essentially the desorption activation energy. Using a value for ΔH that is close to that of water (approximately 17 kcal/mole, a good approximation for unreacted hydrazine [24, p.

696]), the average of the function is taken over the temperature range of -100° and 100° Celsius [39]; values used as part of the “worst-case scenario” methodology. This analysis gives a residence time of about 66 days, and this value is used for further calculations. An important issue to note here is that this value of residence time is only valid for the spacecraft body. The optical instruments are generally kept at much cooler temperatures, and thus a different, longer residence time of about one year is used.

3.5.3 Film Distribution

Having calculated the mass of propellant available to condense on the surface, as well as the time the contaminant will spend there, the thickness of the contaminant film can now be estimated. Generally, this is a very complex problem, and can only be solved using advanced flow analysis. However, some simplifications are made here to give a reasonable estimate. First, it is assumed that the film gets distributed evenly across the entire surface. Obviously this will not be the case; however it works well with the lumped thermal model, where the surface’s absorptance is considered to be constant across the surface. Next, the density of the condensed propellant is taken to match that of water, which is a reasonable assumption for unreacted hydrazine [24, p. 696].

The total mass which will condense on the surface is taken to be the amount of backflow, unreacted propellant expelled over the residence time (66 days). This is split up according to the surface areas of the solar panels and the spacecraft. Using simple geometry and, again, the assumption that the film thickness remains constant over the

surface, the contaminant thickness is estimated. For the optics, a longer residence time is used, but the film thickness is calculated the same way as for the spacecraft body.

3.5.4 Effects

The effects on other subsystems can now be quantified. These effects are mainly optical, and rely on light absorption across the entire spectral range. In this model, empirical relationships found in the literature are used instead. The absorption coefficient of the spacecraft's thermal control material will change, and this change is estimated to be an increase of about 0.01 for every 100 Å of contaminant thickness [9, p. 145]. The power produced by the solar panels will also decrease with an increased contaminant thickness. Tribble [7, p. 57] gives an estimate of a 2% decrease in power output for every μm of contaminant film thickness. These values are calculated, and then used by the appropriate subsystem model for its own analysis.

3.6 Atomic Oxygen Effects

For some spacecraft materials, the presence of atomic oxygen in orbit can pose a problem. This problem is most significant in low Earth orbit, where the concentration of atomic oxygen is highest. The problem is relatively simple: calculate the erosion rate of the thermal control material, and estimate the "lifetime" of the material – the amount of time it takes for the material to completely erode.

The erosion process occurs when atomic oxygen reacts with the material, and the new compound is ejected from the surface. The controlling rate is given by the material's Reaction Efficiency (RE , also known as Erosion Yield). This value is determined from in-orbit tests carried out by either the Space Shuttle, the International Space Station, or the Long Duration Exposure Facility (LDEF) [6, p. 186]. The model uses a database of materials whose RE is determined using the values from Table 3.4 [9, p. 148].

Table 3.4: Reaction efficiencies of various spacecraft thermal control materials [9, p. 148].

Material	Reaction Efficiency [10^{-24} cm ³ /AO atom]
Clear FEP or TFE Teflon	0.05
Polyimide (Kapton)	2.6
Black polyimide	2.5
Gloss white polyurethane paint	0.9
Flat black polyurethane paint	0.9
Gloss black polyurethane paint	4.5

This table gives values for the most commonly used spacecraft materials. Other commonly-used materials not shown on this table have negligible reaction efficiencies [9, p. 148].

The erosion rate is calculated by Equation 3.11 [9, p. 149]:

$$\frac{dx}{dt} = (RE)\phi \quad (3.11)$$

Here ϕ , the atomic oxygen fluence, is the product of the ambient concentration of atomic oxygen and the velocity of the spacecraft. The thickness of the material is represented by x . The model reads the selected material's properties (including thickness and reaction efficiency), and calculates the erosion rate. In many cases, the reaction efficiency of the material is negligible, and thus there is no significant erosion.

It is important to note that this erosion occurs only on the leading surface of the spacecraft – the surface in the ram direction. Because of this, complete erosion may not cause the spacecraft to fail. However, because attitude control is not specified (beyond pointing control for the solar arrays), many surfaces may experience erosion. Therefore, the calculated lifetime is a worst-case scenario.

3.7 Glow

Another effect of atomic oxygen in low Earth orbit is the “glow” phenomenon. While the mechanics are not fully understood, the presence of the neutral atmosphere causes light to be emitted around spacecraft surfaces. This phenomenon has been observed on many unmanned spacecraft, as well as the Shuttle [7, p. 100]. Since the spacecraft being designed in this example has on-board optical instruments, it is important that the possible optical contamination due to spacecraft glow is minimized.

This emission is quantified using the empirical relationship from Papazian [40]:

$$\log B = 7 - (0.0129)H \quad (3.12)$$

Here, B is the brightness of the glow in Rayleighs, and H is the altitude of the spacecraft in kilometers. Since B is given in Rayleighs, it has a dependence on the area projected in the ram direction. Before a simulation run is begun, the altitude is specified in the model. Then, the model calculates the brightness of the glow using Equation 3.12. The amount of glow is then used in an objective function to define the relative overall “performance” of the optics in comparison with other designs. This glow occurs only in the ram

direction of the spacecraft. As a worst-case, the model calculates the glow on the largest face; however, glow may be further minimized with some attitude-control capability.

3.8 Objective Evaluation

This section explains the way the various inputs and outputs for each model are translated into objective values. Again, these values serve to compare the designs with each other, and are not meant to give accurate estimations.

3.8.1 Lifetime

The model provides three different estimates for the lifetime of the spacecraft: the estimate from the solar array section and atomic oxygen sections, as well as an estimate based on propellant budget. The most conservative estimate is given as an output of the model. The atomic oxygen model only contributes to the lifetime of the spacecraft if the thermal control material used has a non-zero reaction efficiency. However, lifetime estimates from the solar array model and the propellant budget calculation are given for every design iteration.

The solar array and atomic oxygen-based lifetime estimates are explained in Sections 3.4 and 3.6, and the estimate based on propellant budget will be explained here. Essentially, this lifetime simply depends on how long the spacecraft can remain in orbit given the amount of propellant it can carry. The total allowable propellant mass is roughly estimated to be 15% of the total spacecraft mass [11, p. 28]. The spacecraft mass

itself is estimated as a function of its volume using the following relationship from Wertz [13, p. 337]:

$$Vol = 0.01 \times Mass \quad (3.13)$$

Given the annual ΔV budget from Section 3.5.1, as well as the total ΔV budget of the spacecraft, a rough lifetime estimate can easily be obtained. It should be noted that while this lifetime estimate technically has units of years, this model does not aim to provide an absolute estimation. Instead, it is the theoretical estimated lifetime, assuming the only inputs are those which are modeled here. As such, the actual lifetime of a given design will likely be significantly lower because of other unmodeled effects. This is not an issue here, however, because this model provides a way to compare different designs, which is all that is needed for this type of problem.

3.8.2 Optics Performance

The optics performance metric is based on two values: the amount of glow (calculated in Section 3.7), and the amount of contaminant buildup on the optical instrument (calculated in Section 3.5). The amount of glow is essentially dependent on the cross-sectional area of the spacecraft, while the contaminant film calculation process is slightly more complicated. These two values are combined in a weighted objective function, which ensures that both have an equal effect on the total value. The resulting value is called GLOW in the model, and it is minimized. It is important to note that the calculated value from the objective function has no real physical significance, but only serves to provide a performance metric against which other designs can be measured.

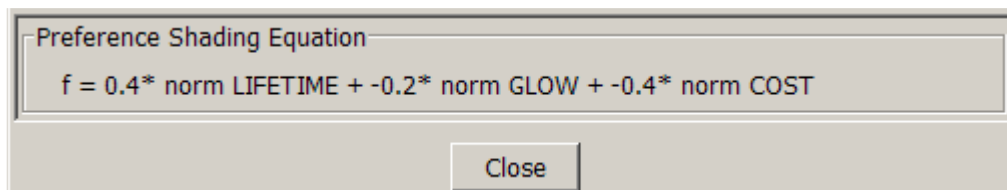
3.8.3 Cost

The cost is simply estimated as a function of total spacecraft mass. Mass is estimated using the relationship in Equation 3.3, and the value is simply normalized to give a cost estimate which scales well. Again, as is the case with the optical performance metric, the resulting value does not represent a true cost estimate, it only provides a way to compare different designs. Cost estimation could warrant its own model, and it is a much more complicated process to accurately estimate the cost of a spacecraft this early in the design phase.

Chapter 4

Analysis

The method ATSV uses to choose preferred designs is a simple weighted objective function. An example objective function generated by ATSV is shown in Figure 4.1. The total cost value f is calculated by multiplying normalized values of each objective by a weighting coefficient. These coefficients are determined from the preference control, and always add up to 1. In the cases explored here, coefficients will be either +/- 0.50, or +/- 0.333, corresponding to equal weightings of two or three objectives. A positive value corresponds to maximizing the objective, and a negative value is used for minimization. It is also noted that the sum of the absolute values of these weights is always one. A designer with different preferences could use ATSV to optimize one or more objectives over another, which would result in different objective weights. This is all done automatically by ATSV depending on the preferences set by the user, who has no direct interaction with the objective function (other than setting the preferences). The value for f is used for quantifying a design's preference value, which is used for visualization and sampling purposes.



Preference Shading Equation

$$f = 0.4 * \text{norm LIFETIME} + -0.2 * \text{norm GLOW} + -0.4 * \text{norm COST}$$

Close

Figure 4.1: Objective function resulting from preference controls set in Figure 4.2.

An important distinction should be made regarding the idea of “best” designs. This model lacks the fidelity to give a single, useful, overall best design; rather, it is meant to provide the user with a set of best designs which may then be further processed with more detailed models. However, in this chapter, “best” designs are defined as the single most preferred solution, chosen by ATSV. Often this design will be found in an area of the trade space that contains a trivially narrow range of objective values, however in order to quantify the results, only the single best design is chosen and documented.

4.1 Objective Sets

The model developed here has a set of three objectives, which ATSV can minimize or maximize with varying degrees. Figure 4.2 shows the control window in which the user can set the different objective weights. The brush controls allow the user to specify the range of acceptable values for each objective, and the preference controls are for setting the relative objective weights. In order to get a complete picture of the design space generated by the model, various objective weights are used for different “runs”.

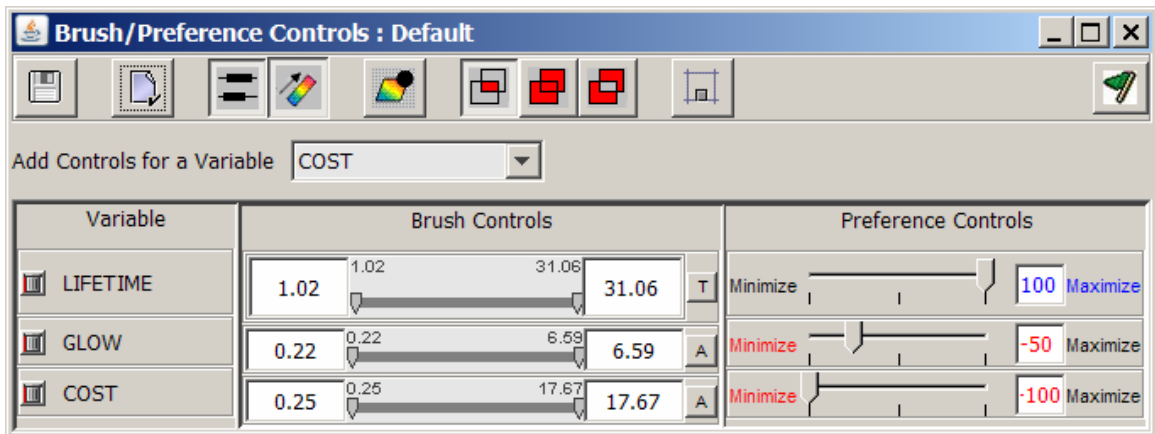


Figure 4.2: ATSV brush preferences control window.

The different sets of objective weights explored here are shown in Table 4.1. Color is used here only to illustrate whether the objective is being maximized (green) or minimized (red). The first three (individual objective optimization) are not likely to be used in any real world scenario, although they can give insight into the absolute extrema of each objective by itself; these runs essentially help to characterize the design space. The last four show combinations involving two or more of the objectives, and are more likely to represent actual desired preferences for a space mission. Different budget constraints, as well as different primary objectives could yield these various combinations. The final run is meant to extremize all three objectives, and especially illustrates the power of ATSV in dealing with multi-dimensional systems. In order to rule out completely egregious designs, runs which do not have a preference on lifetime are set so the minimum lifetime is 6 months.

Table 4.1: Outline of the various objective preference sets explored.

Description	Lifetime	GLOW	Cost
Longest possible lifetime	+100	0	0
Highest quality optics	0	-100	0
Lowest possible cost	0	0	-100
Low cost, high quality optics	0	-100	-100
Long lifetime, high quality optics	+100	-100	0
Long lifetime, low cost	+100	0	-100
Best combination	+100	-100	-100

4.2 Procedure

The same procedure is used for each case, although different visualization tools are used depending on the number of objectives. The design space is initially filled with 200 randomly generated combinations which represent different designs using the Basic Sampler in ATSV. The constraints and preferences are then added. After that, a combination of the Preference Sampler (generations based on objective preferences), Pareto Sampler (designs close to the Pareto frontier), and Attractor Sampler (designs close to some user-specified point in the design space) is used. After narrowing down to a region of interest, ATSV is used to select the best design; and from there the Point Sampler, which holds other variables constant as the user adjusts one variable, is used to find designs close to the space in which the best design occurs. After several iterations, the best point is selected. Generally, ATSV generates 3,000 to 10,000 total designs for each set of objectives.

4.3 Single Objective Optimization

Although using advanced visualization tools to optimize a single objective may seem trivial, it is important to establish “baseline” results for each of the objectives, so later runs may be compared against them. Ideally, each of these individual runs will yield an overall maximum or minimum, which will then be compared to extrema generated from other runs.

4.3.1 Lifetime

The first example run involves finding the maximum lifetime, with no other objective preferences. Figure 4.3 shows the visible designs generated in this case. Units on the vertical axis are generic cost units used by the model, while units on the horizontal axis are years.

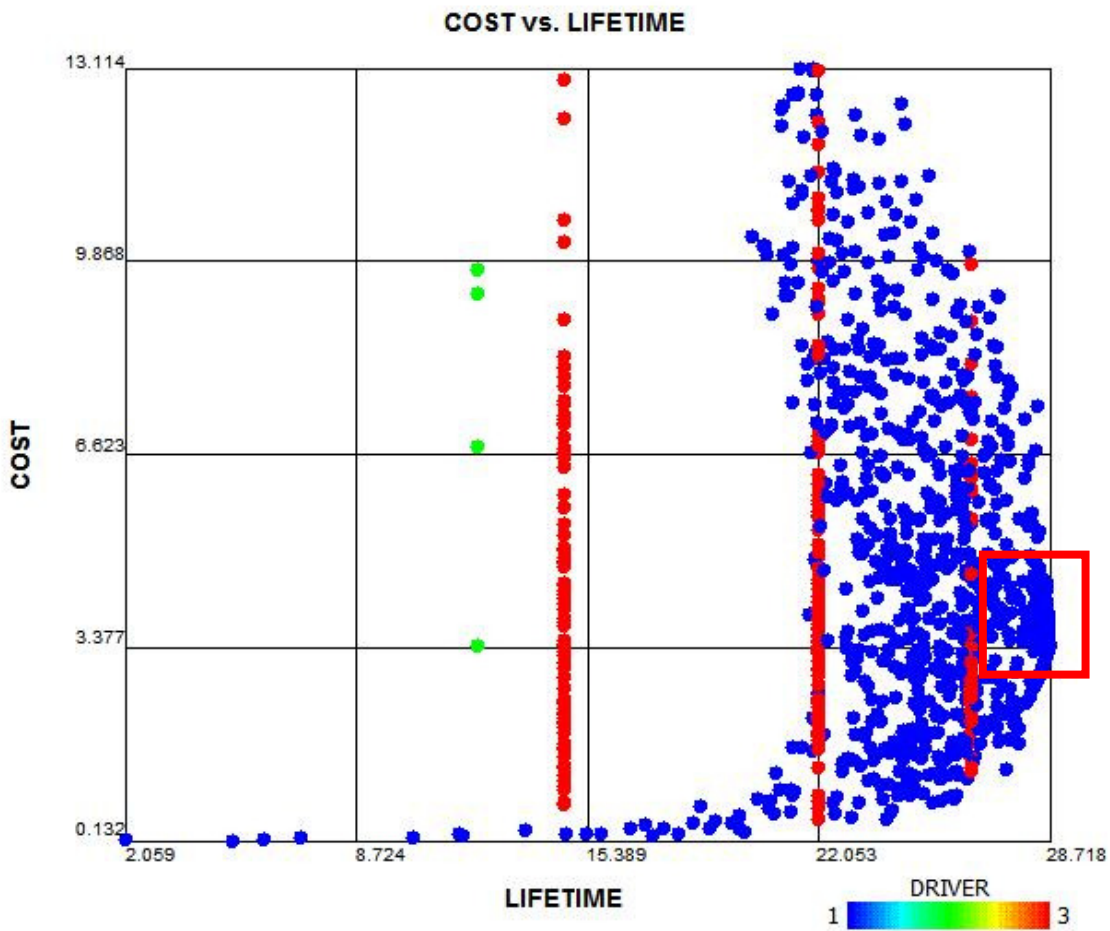


Figure 4.3: Cost vs. Lifetime plot, maximum lifetime case (color showing lifetime driver).

Obviously the preference here is to the right of the plot (longest lifetime), so instead color shows the “driver” of the lifetime model (which subsection produced the lowest lifetime). Blue designs are limited by the solar array, red are limited by atomic amount of propellant, and green are limited by atomic oxygen effects.

It is evident that the solar array model produces the strictest limit on lifetime, since the vast majority of designs are blue. It is also interesting to note the structure of the red designs: discrete columns. These columns correspond to a specific thruster type

(specifically: Hydrazine, H_2O_2 , and HAN-based, left to right). This specific structure is a result of the way the model works: both the amount of propellant and the imparted acceleration from a given thruster are dependant on the spacecraft's mass, so essentially the lifetime estimate ends up being dependant only on the thruster's specific impulse.

A similar structure is evident for the atomic oxygen-limited designs. The reason for this is, as mentioned before, atomic oxygen erodes only certain thermal materials. The green designs correspond to a situation in which the selected material was susceptible to atomic oxygen erosion, and its lifetime estimate happened to be higher than the other two. Both the atomic oxygen and the propellant amount columnar structures appear throughout the analysis.

The area on the plot boxed in red in Figure 4.3 shows our area of interest, since it contains the designs with the highest lifetimes. Figure 4.4 shows a zoomed in view of that densely-populated area. Note that in this plot the color has been modified to show preference, not the lifetime driver. From this view it is easy to choose the best design (circled). The proximity of so many designs in such a close space on the plot is a result of using the Point Sampler tool in ATSV, which essentially finds nearby designs by slightly changing individual variables. Table 4.2 shows the details of the chosen design.

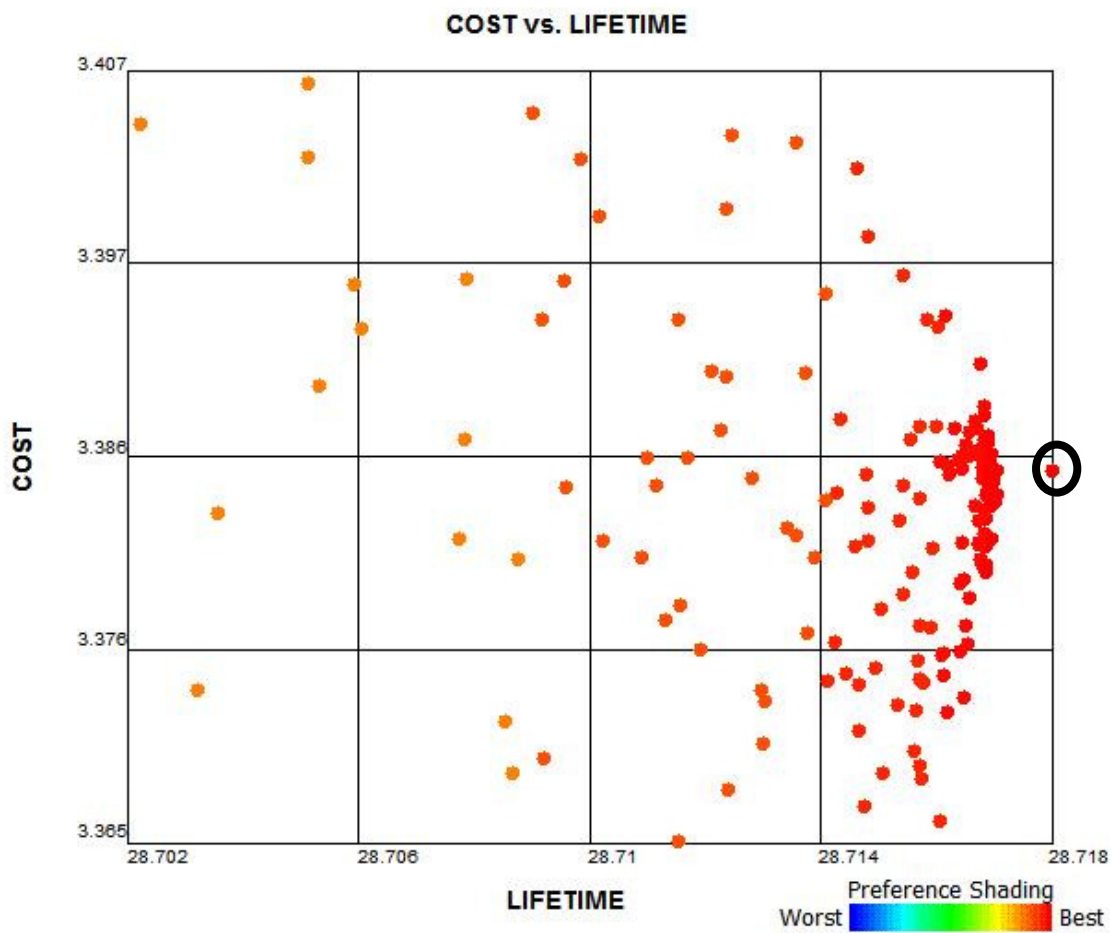


Figure 4.4: Cost vs. Lifetime, maximum lifetime case, zoomed in to the best designs.

Table 4.2: Maximum lifetime design details

Variable	Value
Dimensions	0.55x2.19x2.19 [m]
Thermal material	Aluminized Teflon
Propellant type	O ₂ and RP-1
Lifetime	28.72 [years]
GLOW	1.1883
Cost	3.3854
Lifetime Driver	Solar array

4.3.2 GLOW

This case proved to be slightly less straightforward, in that there was no distinct area of interest which appeared. Instead, there were many designs with very close GLOW values, as can be seen in Figure 4.5 (color used to show preference). This figure shows a parallel coordinates plot. Each axis represents either a design variable or objective, and each individual design is shown as a line intersecting all axes. This allows us to gain insight into the level of diversity among the designs, and what values for each variable tend to yield the preferred designs.

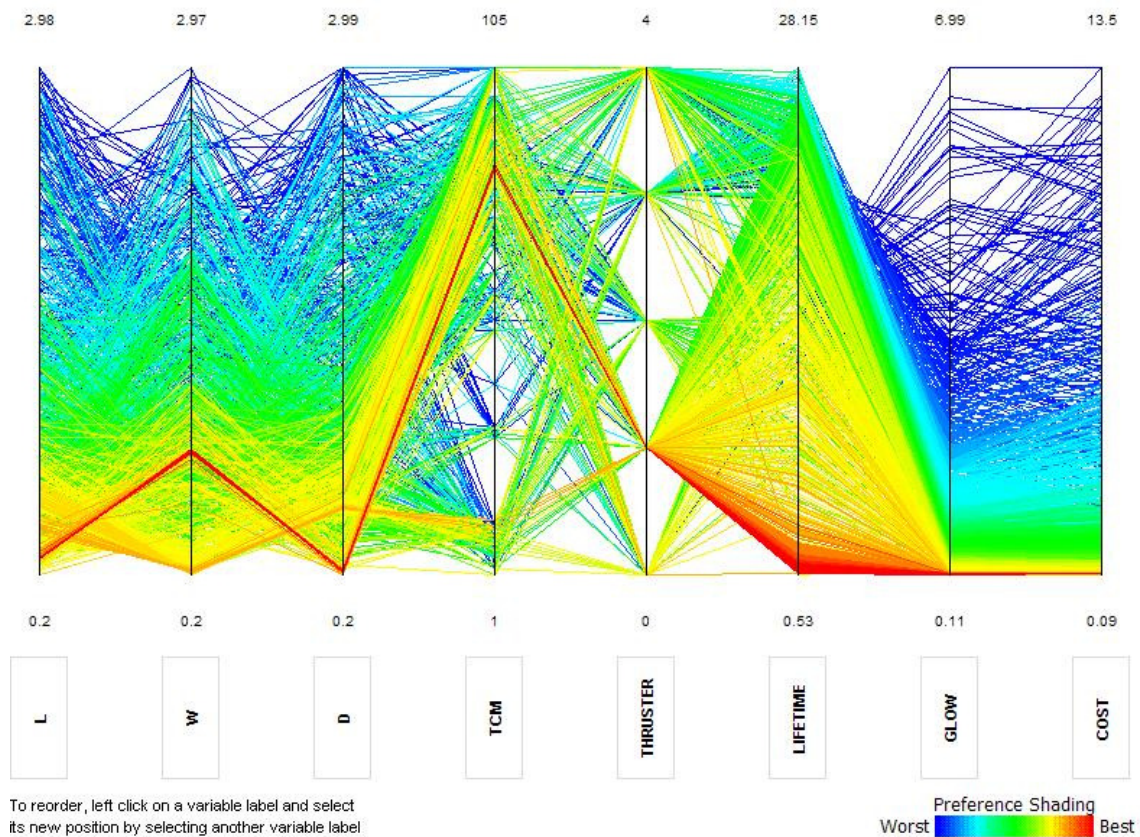


Figure 4.5: Parallel coordinates plot, minimum GLOW case.

Figure 4.6 shows the zoomed view of the area of interest, again with Lifetime on the horizontal axis. It can be noted that this area actually includes a very narrow range of GLOW, and in fact the entire set of best designs falls within a very small margin for each design variable.

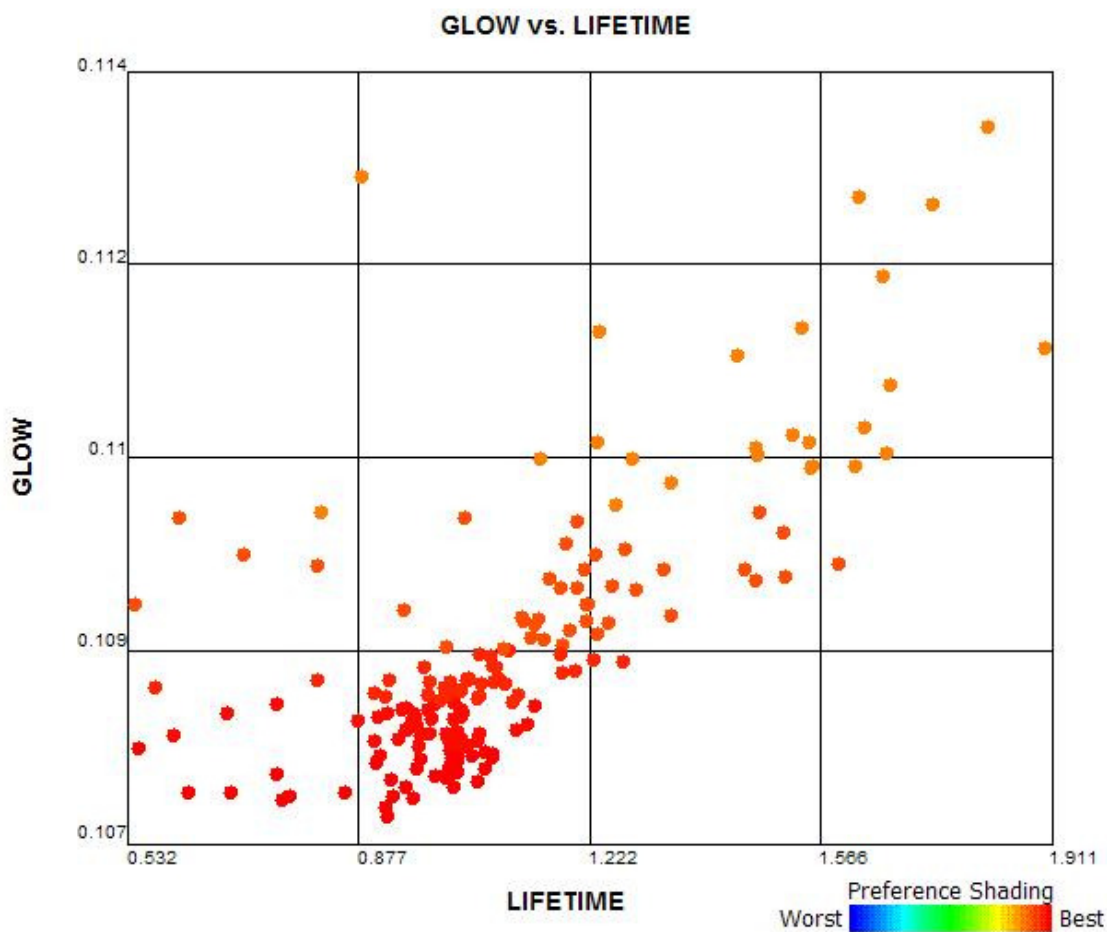


Figure 4.6: GLOW vs. Lifetime plot, zoomed in to area of interest.

One of the reasons there is such an abundance of low-GLOW designs is the objective's dependence on the spacecraft's dimensions: minimizing the cross-sectional area in the ram direction leads to less spacecraft glow. Because of this, the model needs to only produce small (although still valid) designs in order to obtain low GLOW values;

contamination, while still a factor in this objective, fails to significantly influence the design direction here. The design details for the chosen optimal point are given in Table 4.3.

Table 4.3: Minimum GLOW design details

Variable	Value
Dimensions	0.29x0.87x0.22 [m]
Thermal material	MgO AIO Paint
Propellant type	HAN-based
Lifetime	0.625 [years]
GLOW	0.1076
Cost	0.09487
Lifetime Driver	Solar array

4.3.3 Cost

As in the GLOW case, the minimum cost case produced many designs within a small range of objective values. This is again a result of the Cost objective's strong dependence on dimensions of the satellite. The design space is very similar to that of the minimum GLOW case, so individual plots will not be shown for this case. Table 4.4 shows the design details for the lowest-Cost design.

Table 4.4: Minimum Cost design details

Variable	Value
Dimensions	0.35x0.72x0.20 [m]
Thermal material	Aluminized Kimfoil film
Propellant type	HAN-based
Lifetime	0.50 [years]
GLOW	0.1049
Cost	0.0896
Lifetime Driver	Solar array

One notable thing about this design is that it in fact has an even lower GLOW value than the minimum GLOW case. While this is not an encouraging result, the reasoning behind it makes sense; as GLOW is affected by several values (combined into a single objective function), ATSV spends time sampling designs which try to minimize all of these values. Conversely, Cost is affected only by the spacecraft dimensions, so ATSV is able to focus completely on minimizing the dimensions, which in fact lead to a lower GLOW value. Had the user generated more designs for the minimum GLOW case, a better design would have been found. However, the design process was stopped when it appeared ATSV was not making significant progress in minimizing the objective. This illustrates one of the difficulties of user-driven trade space exploration, one which could be rectified by adjusting the way the model calculates the objectives.

Table 4.5 gives the optimal values from these cases, which are used as baselines for the remaining sets.

Table 4.5: Baseline objective values

Objective	Value
Lifetime	28.72 [years]
GLOW	0.1049
Cost	0.0896

4.4 Multi-objective Optimization

Now that the baseline objective values have been found, and the design space has been roughly characterized, the more practical and interesting problem of multi-

dimensional optimization can be explored. These designs are compared with the baseline designs at the end of this chapter.

4.4.1 Low Cost, High Quality

This first case corresponds to an Earth-sensing mission in which long lifetime is not an important factor. Although Lifetime is not being optimized in this problem, a design life can be specified using the brush preferences (six months is used here); designs below this threshold are marked as infeasible. This case is interesting because the two objectives are complimentary to each other – both involve the dimensions of the spacecraft.

Figure 4.7 shows a zoomed view of the area of interest for this case. Color is used to show preference, with red representing more preferred designs.

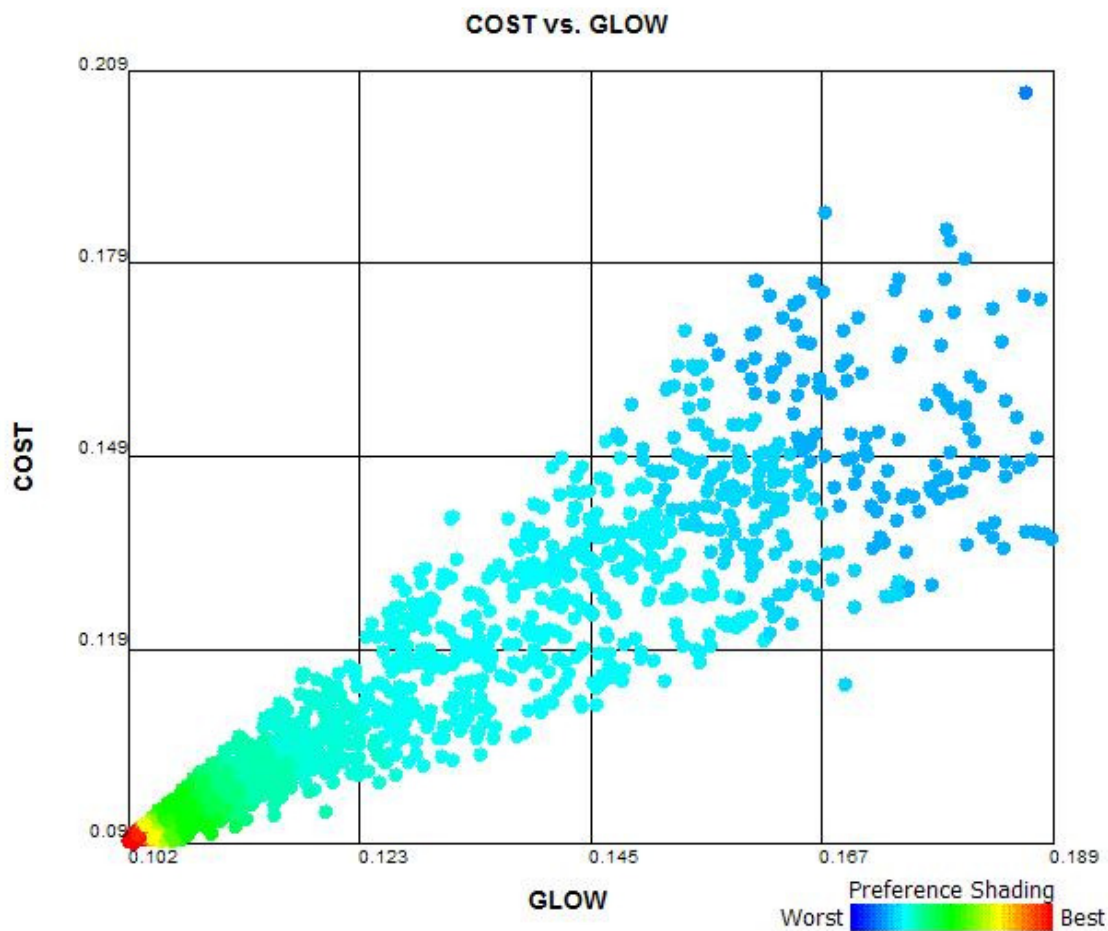


Figure 4.7: Cost vs. GLOW plot, both minimized.

It is evident that there is a high concentration of designs which minimize both of these objectives, as was the case in the individual GLOW and Cost cases. It should also be noted that because of the shared dependencies between these two objectives, adjusting the weights of either objective affects the preferred designs very little. Table 4.6 shows the details for the chosen best design.

Table 4.6: Minimum GLOW, Minimum Cost design details

Variable	Value
Dimensions	0.31x0.80x0.20 [m]
Thermal material	Potassium fluourotitanate white paint
Propellant type	HAN-based
Lifetime	0.628 [years]
GLOW	0.1016
Cost	0.08998
Lifetime Driver	Solar array

It is interesting to note that while the Cost of the selected design is marginally higher than that of the baseline Cost (a result to be expected, since now Cost is not the sole objective), the GLOW of this design is actually lower than the baseline. As was discussed earlier, this is a result of the values ATSV was trying to minimize. This problem, like the GLOW-only problem, relies on the spacecraft dimensions and contamination effects. However, more focus is given to the dimensions because they are involved in *both* GLOW and Cost, while contamination effects only impact GLOW. Therefore, ATSV places more focus on the dimensions, allowing it to generate more designs in the low GLOW area.

4.4.2 Long Lifetime, High Quality

This case, corresponding to a mission with a large amount of funding (corresponding to a higher quality spacecraft with more redundancy), is also of interest. Although every project has budget restrictions, it is interesting to see what the best possible design may be. Also, the designer may see how the designs are affected by adjusting the brush preference for Cost, allowing him to choose the best design for a

given budget constraint. In addition, this allows for an interesting comparison to the three-objective case.

The GLOW vs. Lifetime scatter plot, with preference shading and the Pareto frontier highlighted (Pareto designs marked by the black '+'s), is shown in Figure 4.8. Technically, any designs along this front are preferred for the set of objectives; however, the preference here is towards the bottom right corner of the plot. The Pareto front serves the purpose of allowing the designer to choose either a slightly higher-lifetime design (with lower performance) or vice-versa.

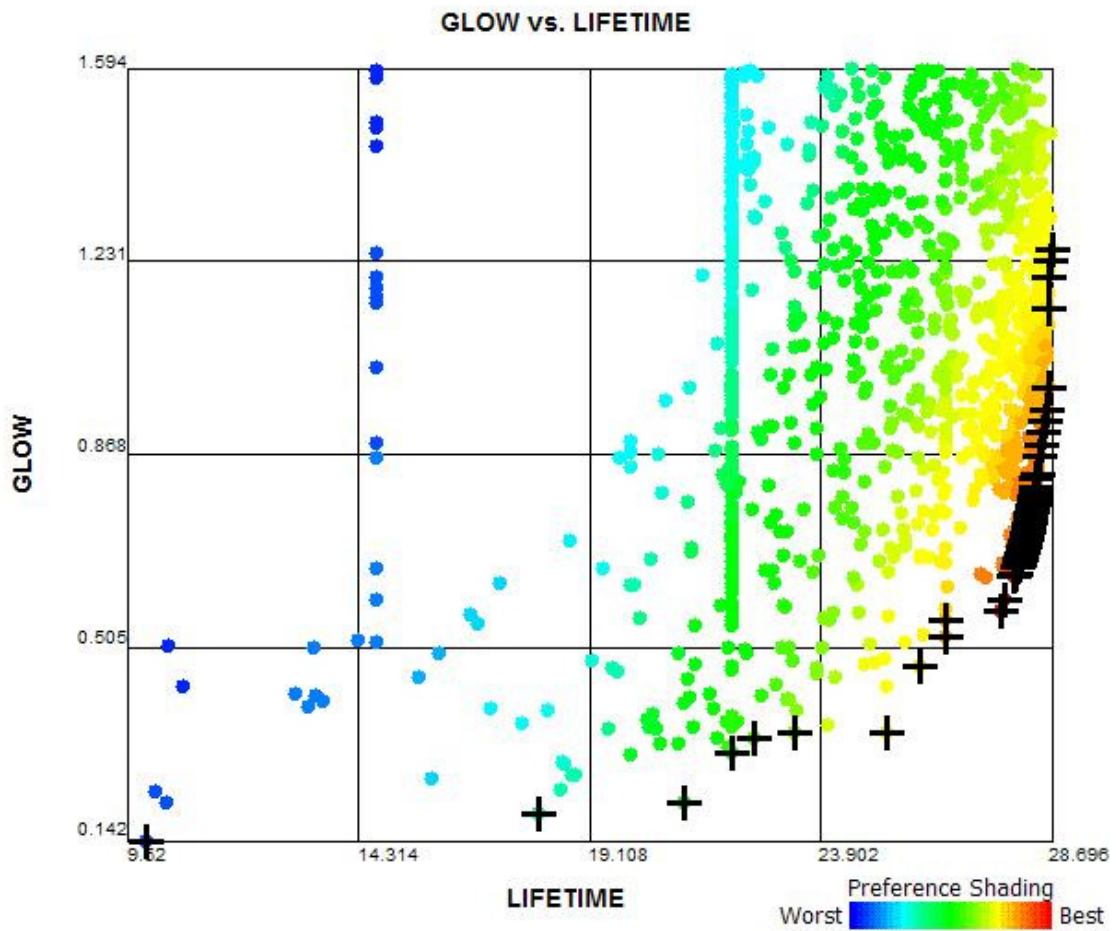


Figure 4.8: GLOW vs. Lifetime scatter plot, high Lifetime and performance case, Pareto front highlighted.

Figure 4.9 shows the level of “diversity” within this particular design space. Preferred designs (shown in red) can be found with a wide range of input variables. Comparing this to Figure 4.5, it is evident that the band of best designs is much wider in this particular case, representing a more diverse acceptable design space. Unlike previous cases, this case has conflicting objective preferences, which makes for a wider range of acceptable designs.

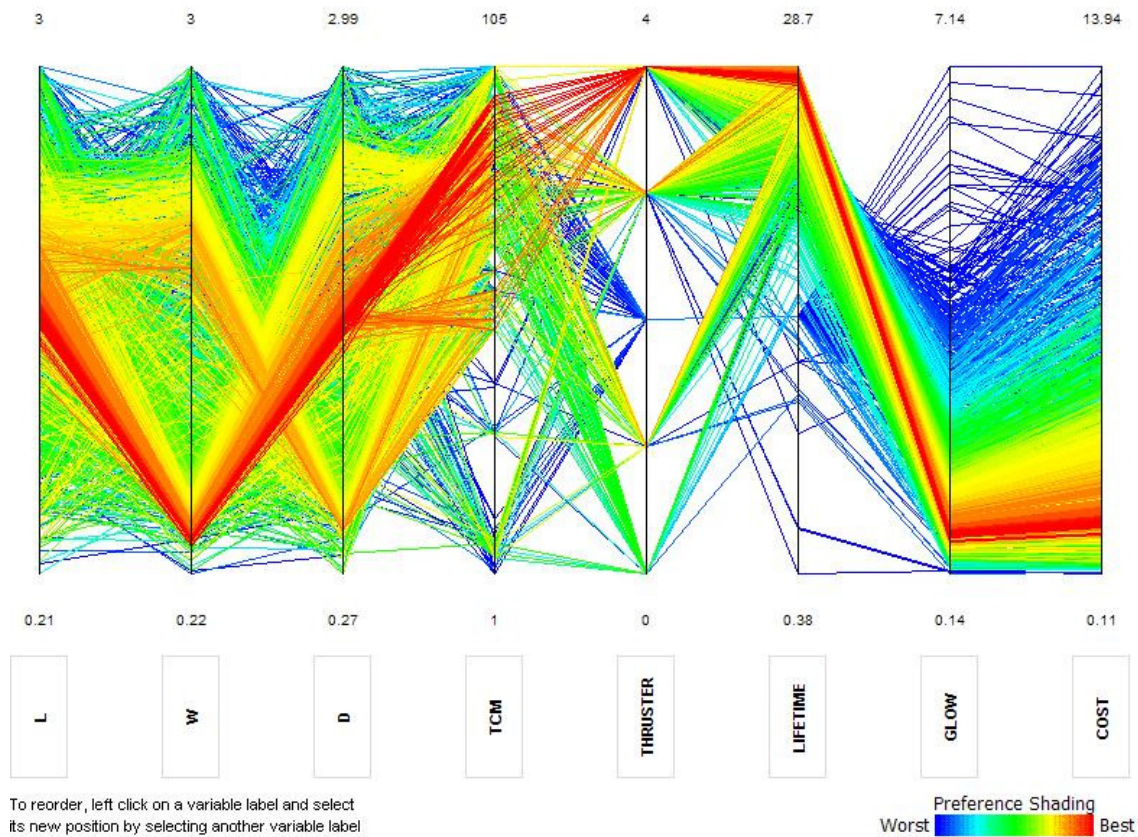


Figure 4.9: Parallel coordinates plot for long life, high performance case.

Before the best design is chosen, it is useful to illustrate the effects of preference brushing on the design space. Figure 4.10 shows the design space after the Cost objective has been tightened by removing the costliest designs.

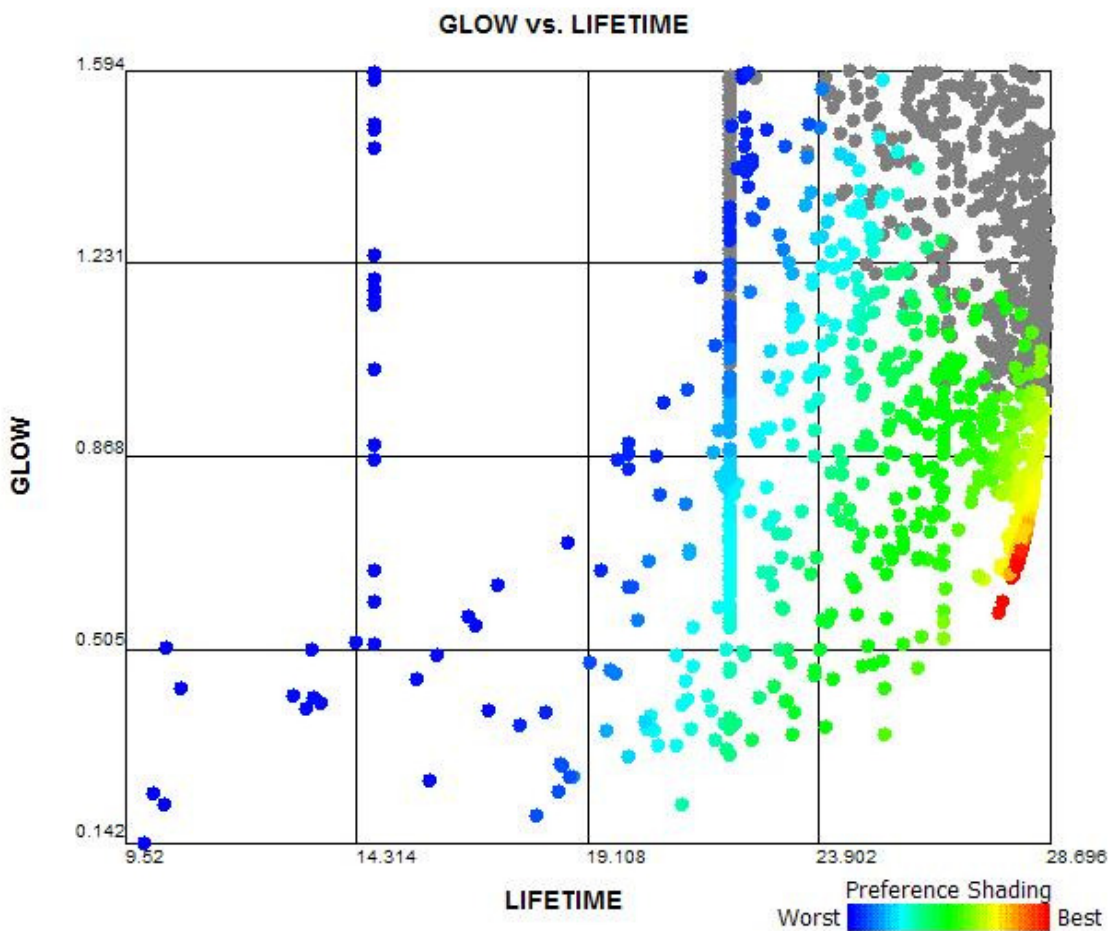


Figure 4.10: GLOW vs. Lifetime, with Cost used as brush preference.

The gray designs are now infeasible, as they have a cost outside the acceptable range. This also affects which designs are considered “best”, as shown by the difference in preference shading between this figure and Figure 4.8. In addition to eliminating designs outside of the acceptable range, the designer may also use this tool to determine the characteristics which contribute to a certain objective.

ATSV was used to select the best design. Characteristics of this design are given in Table 4.7.

Table 4.7: High Lifetime, high performance design details

Variable	Value
Dimensions	1.57x0.39x1.55 [m]
Thermal material	TiO white paint
Propellant type	O ₂ and RP-1
Lifetime	27.95 [years]
GLOW	0.6438
Cost	1.3483
Lifetime Driver	Solar array

Note that although the Lifetime is only slightly lower than the baseline, the GLOW value deviates significantly from its baseline. It is also interesting to note that two of the dimensions are over one meter, whereas previous designs have all been relatively smaller.

4.4.3 Long Lifetime, Low Cost

This case, in which the performance of onboard optics is not as important, parallels the previous case because of the relationship between Cost and GLOW. As such, the process offers very similar results. The Cost vs. Lifetime scatter plot, with Pareto front highlighted, is shown in Figure 4.11.

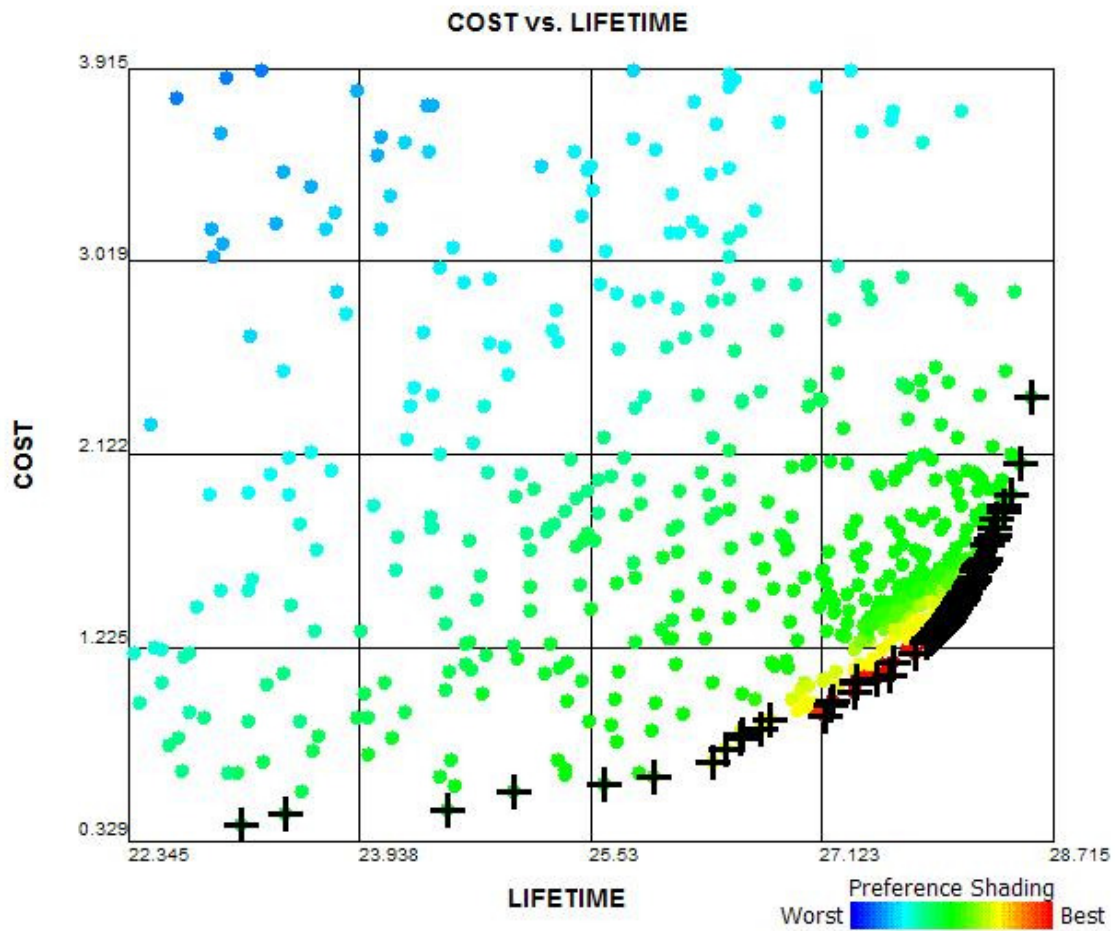


Figure 4.11: Cost vs. Lifetime plot, Pareto designs highlighted.

Again the design space exhibits a clearly defined Pareto frontier. The preference here is to the bottom right corner of the plot, however if the designer wishes to sacrifice lifetime for a lower cost (or vice-versa) he may choose any design along the Pareto front.

Table 4.8 shows that the objective values for this case are in fact very similar to those of the previous case.

Table 4.8: High Lifetime, low cost design details

Variable	Value
Dimensions	1.44x1.44x0.36 [m]
Thermal material	TiO white paint
Propellant type	O ₂ and RP-1
Lifetime	27.59 [years]
GLOW	0.5588
Cost	1.0930
Lifetime Driver	Solar array

It is also very interesting to note that even though these were two separate processes with two different sets of objective weights, the design space was driven to an extremely similar set of variables: the dimensions, thermal material, and propellant type all match (or closely resemble) the values given in Table 4.7.

4.4.4 Optimize All Objectives

In this case all objectives are included: maximum lifetime, minimum GLOW and cost. It is useful here to use three-dimensional visualizations, since any Pareto sets will lay on a surface, not a simply two-dimensional curve. In addition, it should be noted that the best design will rely heavily on user input, and for this case it is chosen by ATSV simply based on the defined objective weights.

This case required a significantly higher number of designs: 17,717 total, of which 7,140 were considered acceptable. One of the main factors contributing to this was a discontinuity in the design space that arose after a few thousand iterations. Figure 4.12 shows this discontinuity in the Cost vs. Lifetime design space.

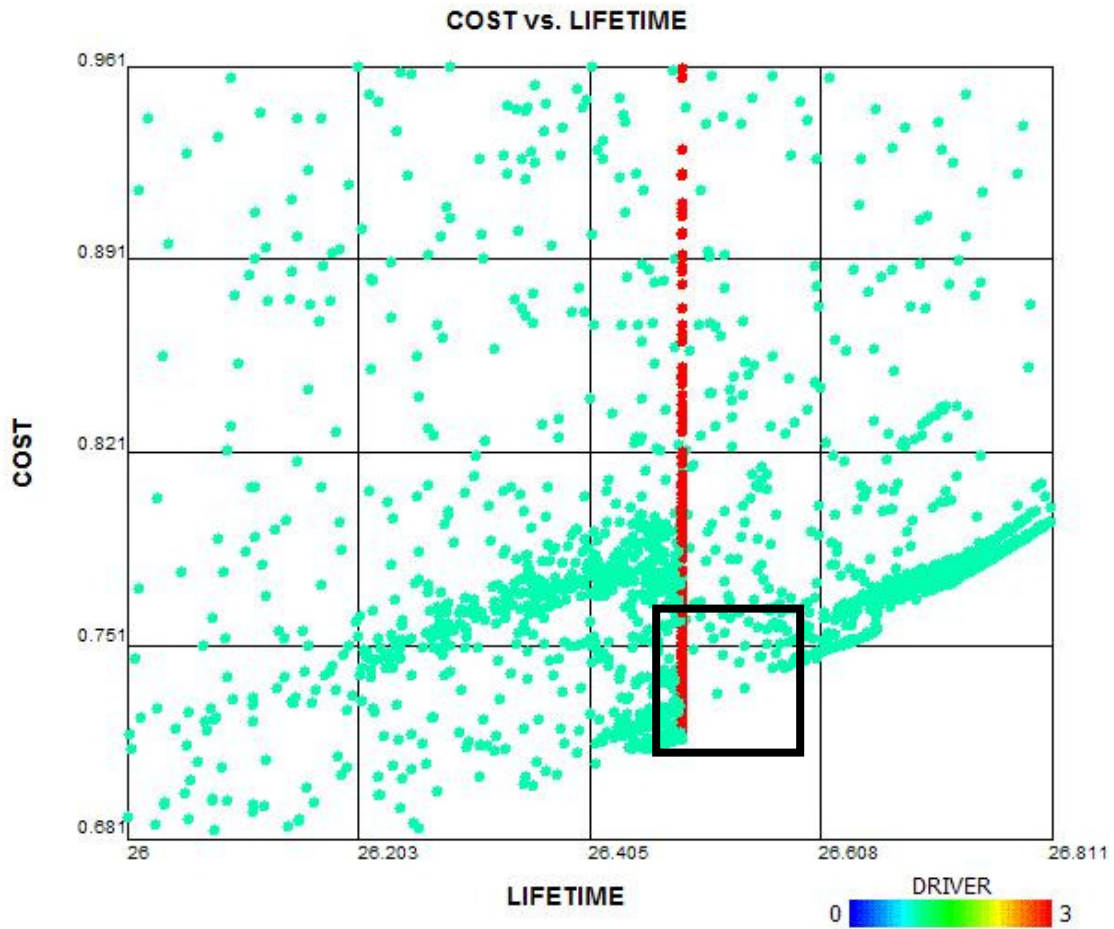


Figure 4.12: Discontinuity in design space, three objective case.

The color here represents the Lifetime driver: the teal colored designs are solar array limited, and the red designs are limited by propellant budget (discussed in Section 4.3.1). By using Point Attractors (which guide the sampler to a particular area of interest), this discontinuity was largely eliminated, however on a finer scale it is still apparent.

The Pareto set is shown highlighted in Figure 4.13. As a result of the dependencies between the Cost and GLOW objectives, the Pareto set is defined along the

edge of the three-dimensional design space. Also note the high concentration of Pareto designs in a small area, a result of the user-driven sampler runs.

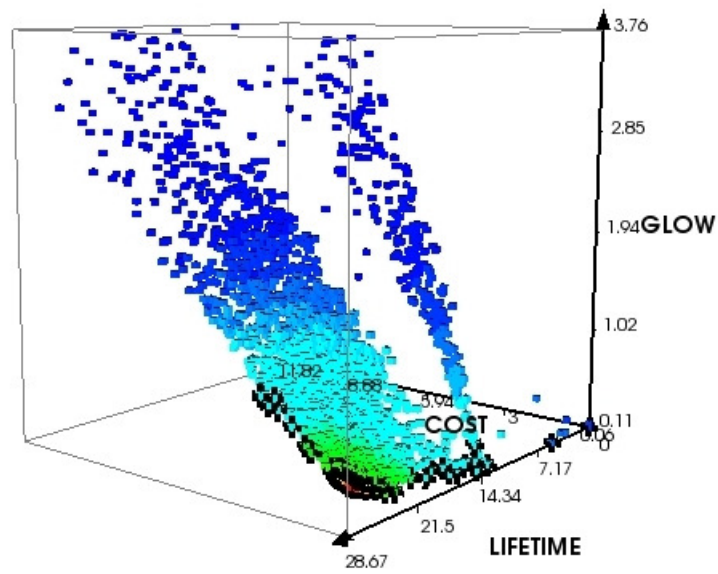


Figure 4.13: Pareto set highlighted, color showing preference.

To better illustrate the position of the propellant budget-caused discontinuity, an isosurface is inserted into the glyph plot in Figure 4.14. Although small discontinuities exist for each propellant type (this particular one corresponds to the HAN-based propellant), this is of interest because it occurs near the area of interest. It can also be noted that this cross-section gives a two-dimensional scatter plot corresponding to the minimum GLOW and cost case in Section 4.4.1.

LIFETIME=26.487

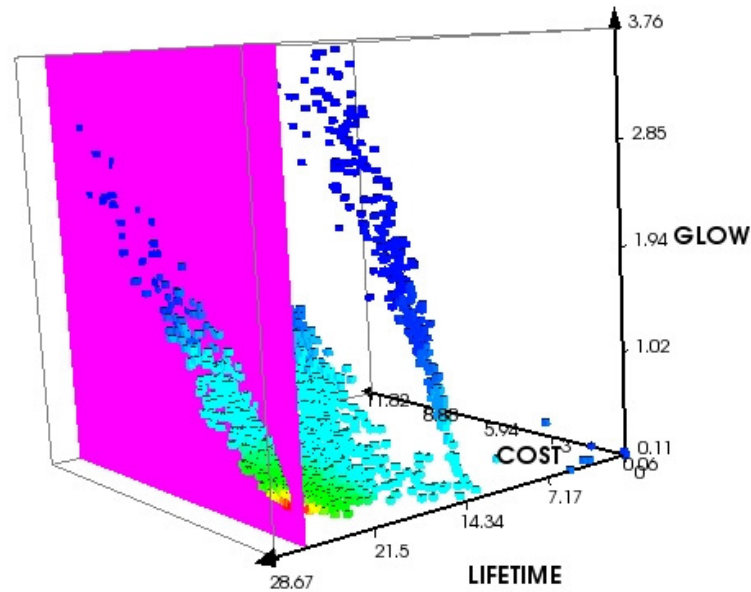


Figure 4.14: Isosurface at propellant budget-caused discontinuity.

Looking at the parallel coordinates plot for this data gives even more insight. For the most part, acceptable designs are spread over a relatively wide range of input variables, as seen in Figure 4.15. The three dimension inputs are of particular interest here: the “best” designs all lie within a range between about 0.3m and 1.4m. In addition, all of the best designs follow the pattern of using two larger dimensions and one smaller dimension (a trend seen in all runs thus far). The reason for this can be traced back to the solar array sizing model and the way GLOW is calculated: the solar array size is proportional to the area of the largest sides of the spacecraft (preference to maximize size), and GLOW is proportional to the area of the spacecraft in the ram direction (taken

to be the smallest face, preference to minimize size). Because of the way the preferences were set, ATSV finds the best trade-off between the two.

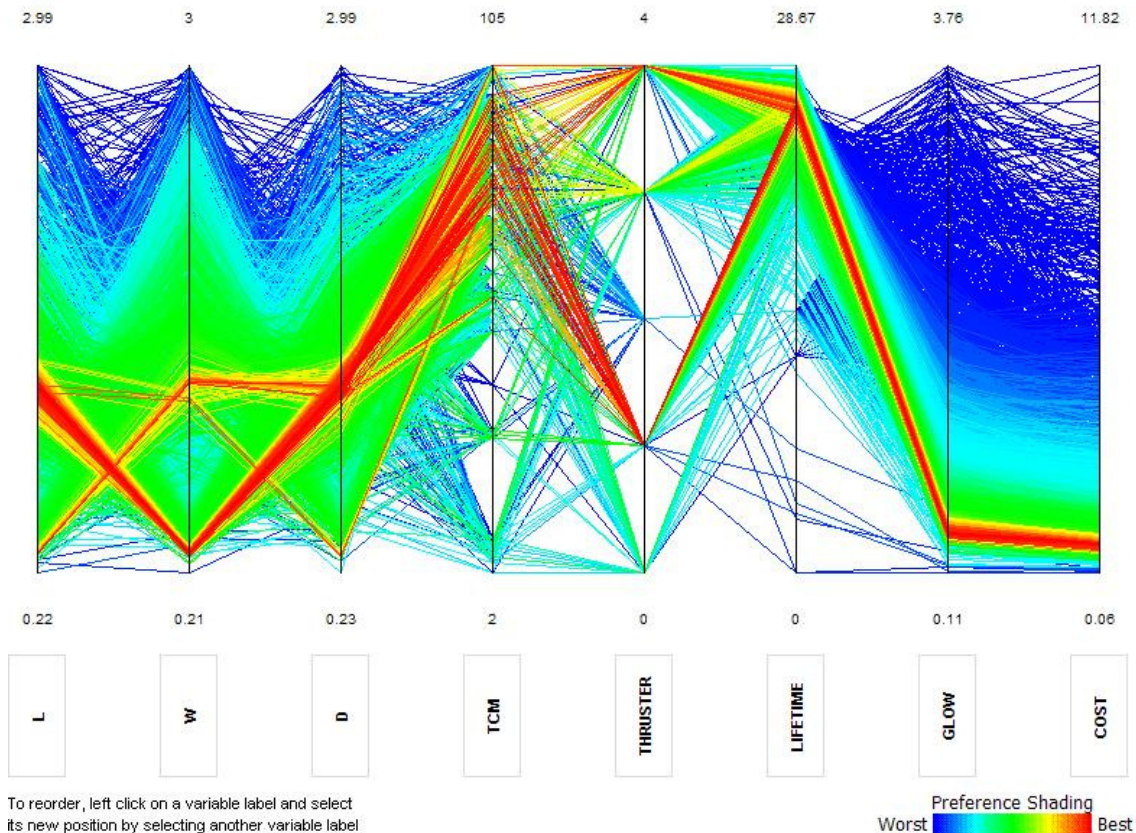


Figure 4.15: Parallel coordinates plot for three-objective case.

Again, this shows that only a certain subset of the thermal control material (TCM) database yields acceptable results (a trend mirrored in Figure 4.9), and while all propellant options yield acceptable designs, only the HAN-based and O₂ and RP-1 propellants produce the best designs.

Table 4.9 gives the details for the best design, which happens to lie near the discontinuity discussed earlier (see Figure 4.16).

Table 4.9: Three-dimensional optimization design details

Variable	Value
Dimensions	1.24x0.31x1.24 [m]
Thermal material	GSFC NS74 (white paint)
Propellant type	HAN-based
Lifetime	26.486 [years]
GLOW	0.39546
Cost	0.71660
Lifetime Driver	Solar array

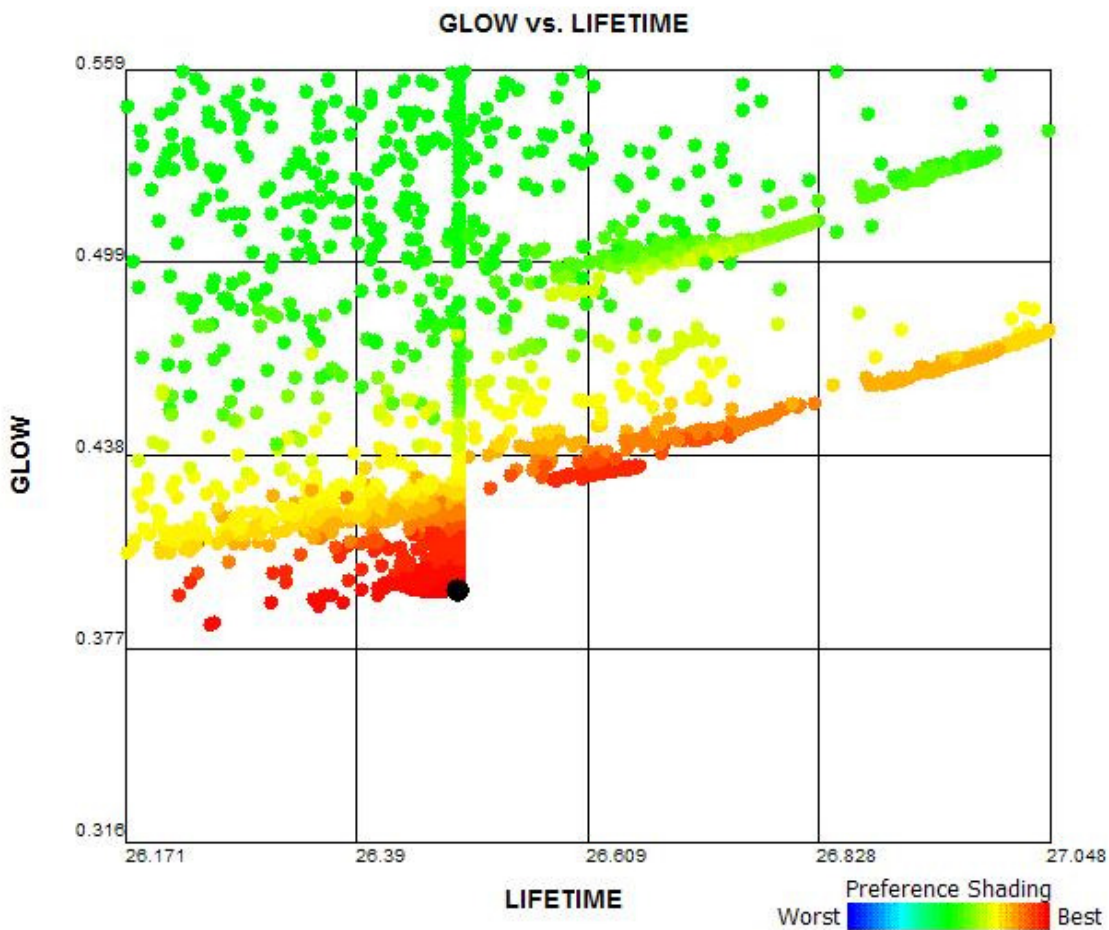


Figure 4.16: Best design highlighted.

4.5 Case Comparison

Comparing the multi-objective cases with the baseline objective values in Table 4.5, neither the Lifetime nor the Cost were optimized beyond the “limit”, although GLOW was further minimized in Case 4. As expected, with the minimization of GLOW and Cost, Lifetime dropped significantly. However, it remained consistently above 25 years for all cases in which it was added as a preference.

Looking at the thermal control materials selected, there is a relatively wide range of acceptable material types. The majority (5) of “best” designs use a type of white paint, although films and tapes also yielded acceptable designs. It is also interesting to note that in most cases, the section of thermal control materials containing black paints yielded very few feasible designs. This is an expected result, since the allowable temperature ranges are relatively low, and power dissipation in the satellite is able to provide most of the required heat. All of the chosen designs are limited by the solar array lifetime, although many designs (even some of those in the Pareto sets) have different drivers, as seen in the final case above. The chosen designs are dominated by HAN-based and O₂/RP-1 propellants, which is an interesting result considering their properties. Neither is the highest or lowest in terms of specific impulse or bulk density, which perhaps is indicative of the trade-offs being made within the model.

Figure 4.17 serves to show the diversity among the thermal control material and propellant selections. Acceptable designs are found for the majority of materials (left axis), and every propellant type (right axis). The gap at the bottom of the TCM axis

corresponds to the lack of designs using black paints, while any gaps on the “thruster” axis occur simply because of the lower number of choices.

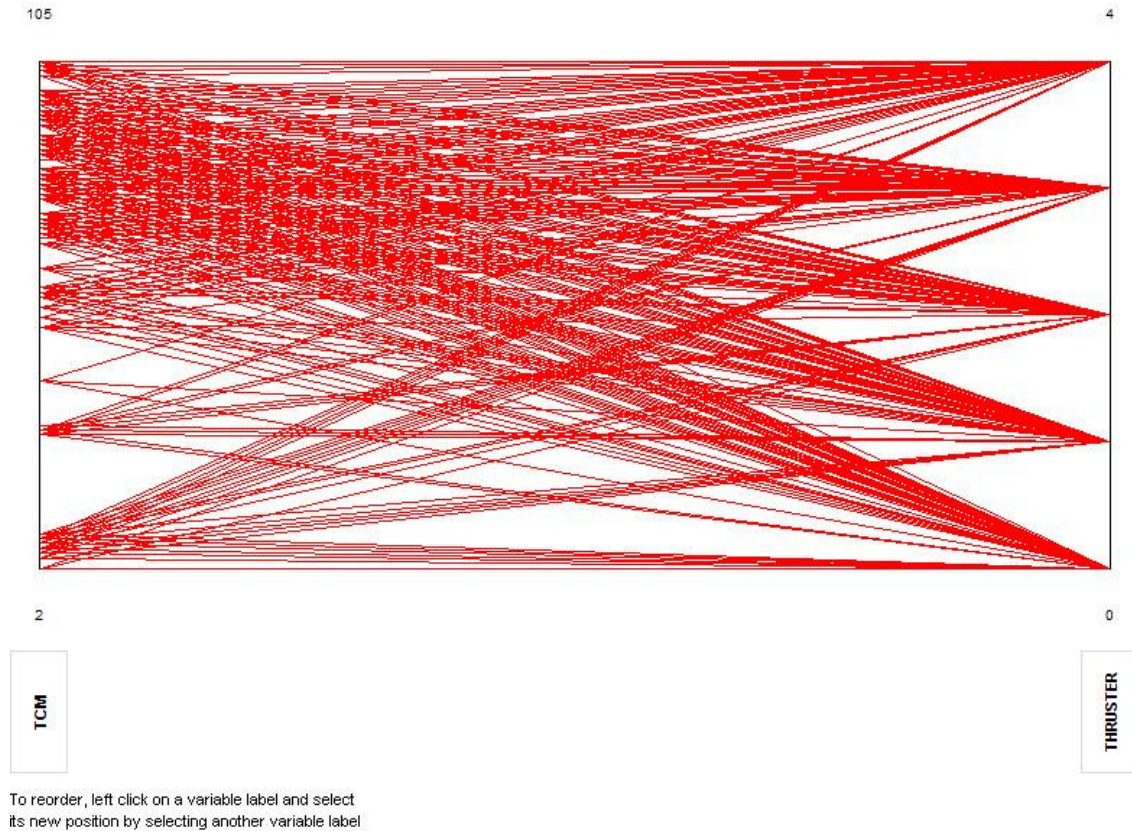


Figure 4.17: Parallel coordinates plot showing the thermal control material and thruster selections.

Figure 4.18 shows trends in Cost, GLOW, and total spacecraft volume over the different runs. With the exceptions of the single objective runs, and the combined minimal GLOW/Cost case, all three values steadily decrease. GLOW decreases more slowly than Cost and volume, a result of that particular objective being dependent on multiple subsections of the model.

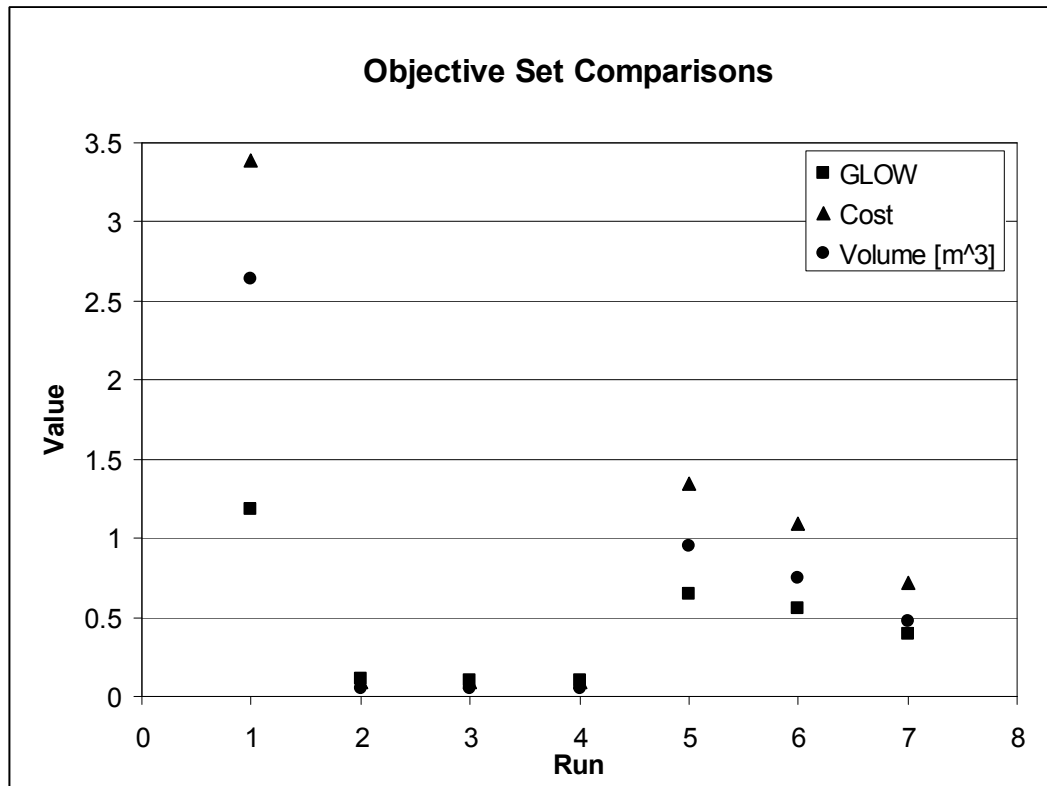


Figure 4.18: Cost, GLOW, and Volume across each objective set.

Chapter 5

Conclusions and Future Work

Overall, this work demonstrated the usefulness of trade space exploration as applied to spacecraft design. The inherent complexity of space systems makes this type of design optimization an ideal fit. While the model developed here has a lower “resolution” or “fidelity” than one which would be used in industry, the principals and methods presented can be scaled and applied to any more detailed model or set of models.

5.1 Conclusions

This work provides yet another example of the power of trade space visualization for highly coupled, complex systems analysis. Because the model outputs are only used to gauge designs relative to each other, it is difficult to compare the designs generated with actual spacecraft designs. However, the model can provide insight into some basic trends in modern spacecraft design.

While the industry pushes towards smaller spacecraft (as mentioned in Chapter 2), so does the model developed here: although the maximum volume of the satellite is restricted at 9 m^3 , all preferred designs converged to a fraction of that (generally less than 30%). Figure 4.18 illustrates this trend within the context of this particular work.

The extremely high number of thermal control materials available for spacecraft (of which only a fraction were used in the model database) is proven not to be excessive: even small changes in their optical or physical properties can make the difference between a feasible and an infeasible design, and useful designs are found across nearly the entire database range. The exception here is the black coating subset of materials; however this is merely a result of the rate of internal heat generation of the spacecraft being sufficiently high as to not require additional absorption via radiation. The black materials could very well be feasible for a different spacecraft.

Similar conclusions can be drawn from the propellant selection: not only are useful designs found for each propellant type used in the model, but the propellants chosen in most feasible designs illustrate the delicate trade-offs that are made in the selection process. Specifically, the two propellant types which occur most frequently in the optimal designs, HAN-based and $O_2/RP-1$, are both “middle of the road” in terms of specific impulse and bulk density (two of the primary properties in this model).

Looking at the lifetime estimate drivers, solar array sizing accounted for the majority of designs. Propellant capacity limits affected a significant number of designs, while atomic oxygen limits the fewest. The latter is likely because only certain types of materials have a non-negligible reaction efficiency; the design space may have been driven to choose those nonreactive materials. Since both propellant capacity and solar array size are determined by the dimensions of the satellite, it can be expected that both play a significant role in the design space.

5.2 Suggestions for Future Work

While this work shows the effectiveness of trade space exploration applied to spacecraft design, there is lots of room for expansion. In the case of ATSV itself, the applications are essentially unlimited. Any situation which involves engineering trades can benefit from this application, and its flexibility means that any computational model can be linked to ATSV with little effort.

In regards to the specific model developed here, expansions in the propellant and materials databases would be useful, as well as adding additional properties (specifically cost) for each entry. While it is a relatively straightforward procedure to vary the operational altitude of the target spacecraft, it was not used as a design variable in this work, which could add another improvement to the model.

The opportunity for using the model developed here in tandem with other spacecraft design models is immediately apparent. Because this is a somewhat higher-level design tool, it could be used to find initially optimal sets of designs, which could then be used with other more specific models. The final result from this process would then be a detailed design or set of designs, with realistic estimates of lifetime, performance, cost, etc.

ATSV could be used to accomplish this in one of two ways. First, a set of models could be developed, each with increasing resolution, until the desired level of detail is obtained. The trade space of each model could be independently analyzed, and the results from the previous session could be used as inputs to the next, more detailed model. Alternatively, one all-encompassing model could be developed, and the designer

could simply use this linked with ATSV to generate viable designs. This second approach would likely be far more difficult to execute, since it would require articulating each relationship between components; which could prove very difficult for a highly complex system such as a spacecraft.

In either case, ATSV would be a useful tool, since its flexibility and ability to visualize several dimensions simultaneously would allow the designer to capture system-level details all the way down to component level details, if needed. It is also important to note that virtually any spacecraft design model, regardless of its components, interface, or programming language, could be incorporated and explored with ATSV. No special consideration needs to be taken in order to develop a model that will work within the program. Essentially, the designer is limited only by the models at his/her disposal.

References

- [1] Jordan, D., 2009, Application of Trade Space Visualization to Discrete and Continuous Complex Dynamical Systems, Master of Science Thesis, Department of Aerospace Engineering, The Pennsylvania State University.
- [2] Balling, R. J., 1999, "Design by Shopping: A New Paradigm?," *Proceedings of the Third World Congress of Structural and Multidisciplinary Optimization*, Buffalo, NY, 295-297.
- [3] Hwang, C. L. and Masud, A. S., 1979, *Multiple Objective Decision Making - Methods and Applications*, New York, NY, Springer-Verlag.
- [4] Stump, G. M., Yukish, M. A. and Simpson, T. W., 2004, "The ARL Trade Space Visualizer: An Engineering Decision-Making Tool," *10th AIAA/ISSMO Multidisciplinary analysis and Optimization Conference*, Albany, NY, AIAA, AIAA-2004-4568.
- [5] Stump, G. M., Simpson, T. W., Yukish, M. and O'Hara, J. J., 2004, "Trade Space Exploration of Satellite Datasets Using a Design by Shopping Paradigm," *IEEE Aerospace Conference*, Big Sky, MT, IEEEAC paper #1039.
- [6] Pisacane, V. L., 2008, *The Space Environment and its Effects on Space Systems*, Reston, VA, American Institute of Aeronautics and Astronautics, Inc.
- [7] Tribble, A. C., 2003, *The Space Environment*, Princeton, NJ, Princeton University Press.
- [8] Sholes, B., Zeller, C. and Matheson, B., 2004, "Hydrazine Thruster Plume Contamination Analysis for the Kepler Photometer," *3rd European Workshop on Hydrazine*, Cagliari, Sardinia, Italy, European Space Agency.
- [9] Gilmore, D. G., 2002, *Spacecraft Thermal Control Handbook*, El Segundo, California, The Aerospace Press.
- [10] Tribble, A. C. and Haffner, J. W., 1990, "Estimates of Photochemically Deposited Contamination on the GPS Satellites," *Journal of Spacecraft and Rockets*, 28(2).
- [11] Brown, C. D., 2002, *Elements of Spacecraft Design*, Reston, VA, American Institute of Aeronautics and Astronautics, Inc.
- [12] Tribble, A. C., Boyadjian, B., Davis, J., Haffner, J. and McCullough, E., 1996, Contamination Control Engineering Design Guidelines for the Aerospace Community, NASA Contractor Report 4740.
- [13] Wertz, J. R. and Larson, W. J., 1999, *Space Mission Analysis and Design*, New York, NY, Springer.
- [14] Bedingfield, K. L., Leach, R. D. and Alexander, M. B., 1996, Spacecraft System Failures and Anomalies Attributed to the Natural Space Environment, NASA Reference Publication 1390.
- [15] Mosher, T., Barrera, M., Bearden, D. and Lao, N., 1998, "Integration of small satellite cost and design models for improved conceptual design-to-cost," *Aerospace Conference, 1998. Proceedings., IEEE*, 97-103 vol.3.

- [16] Gubby, R. and Evans, J., 2002, "Space environment effects and satellite design," *Journal of Atmospheric and Solar-Terrestrial Physics*, 64(16), 1723-1733.
- [17] Tai, A. T., Alkalai, L. and Chau, S. N., 1999, "On-Board Preventative Maintenance: A Design-Oriented Analytic Study for Long-Life Applications," *Performance Evaluation*, 35, 215-232.
- [18] Fukunaga, A. S., Chien, S. and Mutz, D., 1997, "Automating the process of optimization in spacecraft design," *IEEE Aerospace Conference*, Aspen, CO, IEEE, 411-427 vol. 4.
- [19] Lee, C. H. and Cheung, K.-M., 2008, "Communication-centric Spacecraft Design Optimization Tool and its Application to the Lunar Relay Satellite Design," *IEEE Aerospace Conference*, Big Sky, MT, IEEE, March 1-8, 2008, 10.1109/AERO.2008.452667.
- [20] Mosher, T., 1998, "Spacecraft Design Using a Genetic Algorithm Optimization Approach," *IEEE Aerospace Conference*, Big Sky, MT, IEEE, March 21-28, 1998, 10.1109/AERO.1998.685783.
- [21] Arbinger, C., D'Amico, S. and Eineder, M., 2003, "Precise Ground-In-The-Loop Orbit Control for Low Earth Observation Satellites," *18th International Symposium on Space Flight Dynamics*, Munich, Germany.
- [22] D'Amico, S., Montenbruck, O., Arbinger, C. and Fiedler, H., 2005, "Formation Flying Concept for Close Remote Sensing Satellites," *15th AAS/AIAA Space Flight Mechanics Conference*, Copper Mountain, CO, AAS 05-156.
- [23] 2006, Delta II Payload Planners Guide. Littleton, Colorado, United Launch Alliance.
- [24] Humble, R. W., Henry, G. N. and Larson, W. J., 1995, *Space Propulsion Analysis and Design*, New York City, NY, McGraw-Hill.
- [25] Brogren, M., Harding, G. L., Karmhag, R., Ribbing, C. G., Niklasson, G. A. and Stenmark, L., 2000, "Titanium-aluminum-nitride coatings for satellite temperature control," *Thin Solid Films*, 370(1-2), 268-277.
- [26] Tsai, J.-R., 2004, "Overview of Satellite Thermal Analytical Model," *Journal of Spacecraft and Rockets*, 41(1), 120-125.
- [27] Colombo, G., Grasselli, U., De Luca, A., Spizzichino, A. and Falzini, S., 1997, "Satellite power system simulation," *Acta Astronautica*, 40(1), 41-50.
- [28] Muraoka, I., Galski, R. L., de Sousa, F. L. and Ramos, F. M., 2006, "Stochastic Spacecraft Thermal Design Optimization with Low Computational Cost," *Journal of Spacecraft and Rockets*, 43(6).
- [29] Messenger, S. R., Summers, G. P., Burke, E. A., Walters, R. J. and Xapsos, M. A., 2001, "Modeling solar cell degradation in space: A comparison of the NRL displacement damage dose and the JPL equivalent fluence approaches," *Progress in Photovoltaics: Research and Applications*, 9(2), 103-121.
- [30] Sackett, L. L., Malchow, H. L. and Edelbaum, T. N., 1975, *Solar Electric Geocentric Transfer with Attitude Constraints: Analysis*. Cambridge, MA, NASA.
- [31] Kerslake, T. W. and Hoffman, D. J., 1999, "Performance of the MIR Cooperative Solar Array After 2.5 Years in Orbit," *SAE 34th Intersociety Energy Conversion Engineering Conference*, Vancouver, British Columbia, Canada, August 1-5, 1999, SAE 99-01-2632.

- [32] Kelley, J. G., 1992, Control of On-Orbit Contamination for the ARGOS (P91-1) Satellite, Rockwell International.
- [33] Schilling, J. H., Spanjers, G. G., Bromaghim, D. R. and Johnson, L. K., 2002, "Solar Cell Degradation During the 26-Kilowatt Electric Propulsion Space Experiment Flight," *Journal of Propulsion and Power*, 18(4).
- [34] Harvey, G. A., 2000, "Thruster residues on returned Mir solar panel," *Optical Systems Contamination and Degradation II: Effects, Measurements, and Control*, San Diego, CA, USA, SPIE, 41-46.
- [35] Rodriguez, G. E., Studer, P. A. and Baer, D. A., 1983, Assessment of Flywheel Energy Storage for Spacecraft Power Systems, NASA Technical Memorandum. Greenbelt, Maryland, Goddard Space Flight Center.
- [36] Fatemi, N. S., Pollard, H. E., Hou, H. Q. and Sharps, P. R., 2000, "Solar Array Trades Between Very High-Efficiency Multi-Junction and Si Space Solar Cells," *IEEE PVSC*, Anchorage, Alaska, September 17-22, 2000.
- [37] Bauer, F., Bristow, J., Folta, D., Hartman, K. and Quinn, D., 1997, "Satellite formation flying using an innovative autonomous control system (AutoCon) environment," *AIAA Guidance, Navigation, and Control Conference*, New Orleans, LA, AIAA-97-3821.
- [38] Bowman, B. R., 2002, "True Satellite Ballistic Coefficient Determination for HADSM," *AIAA/AAS Astrodynamics Specialist Conference and Exhibit*, Monterey, CA, AIAA, August 5-8, 2002, AIAA 2002-4887.
- [39] de Groh, K. K. and Smith, D. C., 1997, "Investigation of the Teflon FEP Embrittlement on Spacecraft in Low Earth Orbit," *7th International Symposium on Materials in a Space Environment*, Toulouse, France, NASA, June 16-20, 1997, NASA Technical Memorandum 113153.
- [40] Papazian, H. A., 1987, "Spacecraft Glow," *Journal of Spacecraft and Rockets*, 24(6), 565-567.